Development of the hyolaryngeal architecture in horseshoe bats: insights into the evolution of the pulse generation for laryngeal echolocation

Taro Nojiri[1*] , Masaki Takechi[1,2] , Toshiko Furutera[1,2] , Nicolas L. M. Brualla[3] , Sachiko Iseki[2], Dai Fukui[4] , Vuong Tan Tu[5,6] , Fumiya Meguro[7] and Daisuke Koyabu[2,3,7*]

Abstract

Background The hyolaryngeal apparatus generates biosonar pulses in the laryngeally echolocating bats. The cartilage and muscles comprising the hyolarynx of laryngeally echolocating bats are morphologically modified compared to those of non-bat mammals, as represented by the hypertrophied intrinsic laryngeal muscle. Despite its crucial contribution to laryngeal echolocation, how the development of the hyolarynx in bats differs from that of other mammals is poorly documented. The genus *Rhinolophus* is one of the most sophisticated laryngeal echolocators, with the highest pulse frequency in bats. The present study provides the first detailed description of the three-dimensional anatomy and development of the skeleton, cartilage, muscle, and innervation patterns of the hyolaryngeal apparatus in two species of rhinolophid bats using micro-computed tomography images and serial tissue sections and compares them with those of laboratory mice. Furthermore, we measured the peak frequency of the echolocation pulse in active juvenile and adult individuals to correspond to echolocation pulses with hyolaryngeal morphology at each postnatal stage.

Results We found that the sagittal crests of the cricoid cartilage separated the dorsal cricoarytenoid muscle in horseshoe bats, indicating that this unique morphology may be required to reinforce the repeated closure movement of the glottis during biosonar pulse emission. We also found that the cricothyroid muscle is ventrally hypertrophied throughout ontogeny, and that the cranial laryngeal nerve has a novel branch supplying the hypertrophied region of this muscle. Our bioacoustic analyses revealed that the peak frequency shows negative allometry against skull growth, and that the volumetric growth of all laryngeal cartilages is correlated with the pulse peak frequency.

Conclusions The unique patterns of muscle and innervation revealed in this study appear to have been obtained concomitantly with the acquisition of tracheal chambers in rhinolophids and hipposiderids, improving sound intensity during laryngeal echolocation. In addition, significant protrusion of the sagittal crest of the cricoid cartilage and the separated dorsal cricoarytenoid muscle may contribute to the sophisticated biosonar in this laryngeally echolocating lineage. Furthermore, our bioacoustic data suggested that the mineralization of these cartilages underpins

*Correspondence:
Taro Nojiri
nojiri0805@gmail.com
Daisuke Koyabu
dsk8evoluxion@gmail.com
Full list of author information is available at the end of the article

the ontogeny of echolocation pulse generation. The results of the present study provide crucial insights into how the anatomy and development of the hyolaryngeal apparatus shape the acoustic diversity in bats.

Keywords Bats, Laryngeal echolocation, Hyolarynx, Trachea, Bioacoustics

Background

Vocalization in mammals shows extraordinary acoustic and functional diversity, leading to remarkable diversity in life histories. Among mammals, the mode of sound production varies with feeding strategy [1], habitat [2], and social behavior [3]. The enormous diversity of sound peculiarities such as frequency, intensity, and duration has been attributed to morphological changes in the sound-producing organ, the hyolaryngeal apparatus, as reported in koalas [4], ungulates [5], primates [6–12], manatees [13], rodents [14–18], and bats [19, 20]. Structural simplification of the larynx and laryngeal descent results in vocal complexity in humans [12]. This evidence provides strong support for the idea that variations in mammalian sound signals are shaped by drastic changes in hyolaryngeal anatomy.

Bats, which generate a biosonar sound with vocal folds, laryngeal cartilage, and intrinsic laryngeal muscles for foraging and navigation (laryngeal echolocation), are ideal to explore the link between hyolaryngeal anatomy and bioacoustics. Phylogenetically, extant bats comprise two groups: Yinpterochiroptera (yinpterochiropterans) and Yangochiroptera (yangochiropterans) [21]. Yinpterochiroptera comprises two lineages: Rhinolophoidea (rhinolophoids) and Pteropodidae (pteropodids). Among these, rhinolophoids and yangochiropterans employ laryngeal echolocation [22]. No pteropodids are capable of laryngeal echolocation, but a handful of pteropodid species are known to employ non-laryngeal echolocation using tongue clicks [23] or wing flapping [24]. The yangochiropterans emit biosonar sounds through the oral cavity, except for Phyllostomidae (phyllostomids) and Nycteridae (nycterids), whereas the rhinolophoids, phyllostomids, and nycterids emit biosonar sounds through the nostril by adjusting the acoustic properties of the nose leaf at the snout [25]. Members of yinpterochiropteran families Rhinolophidae (rhinolophids), Hipposideridae (hipposiderids), Rhinopomatidae (rhinopomatids), and yangochiropteran families Nycteridae (nycterids) and Emballonuridae (emballonurids) also possess two pairs of novel sound-modifying organs, known as tracheal chambers, at the lateral and dorsal sides of the tracheal rings [26–28]. This functions as a Helmholtz resonating amplifier to improve sound intensity, possibly contributing to the emission of echolocation pulses through the nostrils [26, 29, 30]. In contrast to other clades that use nasophonation, members of Rhinolophidae and Hipposideridae

employ Doppler shift compensation (DSC), which allows them to accurately localize targets by adjusting the sound frequency of ongoing signals to fit them within the most suitable frequency for the primary auditory cortex [31]. For this reason, the rhinolophids and hipposiderids are considered to possess one of the most sophisticated echolocation systems among bats [22].

Previous studies on the evolution of laryngeal echolocation have exclusively focused on auditory organs [32–41]. The cochlea, which transmits sound signals to the cerebral system in vertebrates, is one of the most iconic organs because it is markedly enlarged in laryngeally echolocating bats [32]. In addition, laryngeally echolocating bats possess a fully ossified stylohyal attached to the ectotympanic bone, which improves their sensitivity to ongoing signals [34, 42]. The morphology and development of these features have been well-documented in the context of the evolutionary origins of laryngeal echolocation in bats [31, 32, 35–38, 41, 42]. The enlarged inner ear and ectotympanic-stylohyal unit develop heterotopically and heterochronically in rhinolophoids and yangochiropterans, supporting the multiple-origin hypothesis of laryngeal echolocation in bats [39]. The auditory organs for perceiving echolocation pulses have undergone independent developmental changes, presumably reflecting the differences in biosonar pulse emissions among bats.

Concerning the sound-producing organs of bats, a few studies have reported the musculoskeletal morphology of the hyolaryngeal apparatus in adults [26, 40, 43–49]. Laryngeally echolocating bats possess hypertrophied intrinsic laryngeal muscles supported by reinforced cricoid, thyroid, and arytenoid cartilage [26, 44, 50–52]. In particular, the cricothyroid muscle is a superfast muscle essential for the generation of high-frequency sounds in yangochiropterans [19]. Given that the laryngeal cartilage associated with these muscles is gradually mineralized after birth [28, 46, 48], it is predicted that the ontogeny of biosonar pulse emission is linked to laryngeal growth [47]. However, the paucity of our knowledge on the development of the entire anatomy of the hyolaryngeal apparatus and the acoustic peculiarities of the echolocation pulse restrict our understanding of how morphological changes in the vocal apparatus shape the echolocation pulse during ontogeny.

The laryngeal cartilages serve as the support organ between the hyoid and trachea, anchoring the intrinsic laryngeal muscles essential for vocalization. Previous study

on laboratory mice revealed that the size of the cricoid, thyroid, arytenoid, and epiglottic cartilages have been shown to significantly vary with mean fundamental frequency [15]. In the case of the laryngeally echolocating bats, furthermore, due to the mechanical stress by the superfast muscle contraction, the cricoid cartilage of the phyllostomids is calcified in the postnatal individual with immature flight and laryngeal echolocation [48]. Given these facts, it is expected that postnatal calcification of the laryngeal cartilages would improve the sound frequency in mammals. It should be noted that rats and mice also employ the ultrasonic vocalizations (USVs) [53], but unlike laryngeally echolocating bats, they do not possess the superfast muscle in their larynx. Thus, the postnatal calcification dynamics of the laryngeal cartilages are predicted to be qualitatively deviated in laryngeally echolocating bats against mice.

Here, we conducted the first detailed description of the pre- and postnatal development of the hyolaryngeal apparatus and compared morphological development and pulse ontogeny in horseshoe bats (the genus *Rhinolophus*). The hyolarynx was visualized three-dimensionally using micro-computed tomography (micro-CT). In addition, using a diffusible iodine-based contrast-enhanced micro-CT technique (DiceCT) [54, 55], we described the morphology of laryngeal cartilage and intrinsic laryngeal muscles in detail for the first time in bats. Using immunohistochemistry, we described the three-dimensional morphology of the cartilage, muscles, and the innervation patterns of the hyolaryngeal complex. To validate the anatomical peculiarities of bats against other mammals, we compared the hyolaryngeal development of horseshoe bats with that of laboratory mice (*Mus musculus*). Due to the similar body size to the horseshoe bats examined here and previous broad applications for studying laryngeal maturation and disorder [56], the laboratory mouse is an ideal outgroup for the comparative embryology of the hyolaryngeal apparatus. Furthermore, we measured the maximum frequency of each harmonic pulse, CF_1, and CF_2, from postnatal day 0 to adult individuals and compared pulse ontogeny with morphological development. Our study highlights the unique anatomical and developmental patterns of the laryngeal cartilage, cricothyroid muscle, and cranial laryngeal nerve in laryngeally echolocating bats, providing tangible insights into how the anatomy and development of the hyolarynx shape the acoustic diversity in bats.

Results
General morphology of the hyolaryngeal complex in horseshoe bats
Hyoid
The hyoid apparatus of horseshoe bats consists of five bony elements: basihyal, thyrohyal, ceratohyal, epihyal, and stylohyal, whereas in mice, it includes only three elements: basihyal, epihyal, and stylohyal (Fig. 1). In horseshoe bats, the basihyal and thyrohyal bones were fully fused, and the boundary was not evident (Fig. 1A). The epihyal and stylohyal bones were proportionally elongated compared with those in mice. There was a large gap between the basihyal bone and thyroid cartilage, unlike in mice (Fig. 1D, H). The thyrohyoid bone of mice is connected to the thyroid cartilage only by the thyrohyoid muscle attached to the ventral side of the basihyal and rostrolateral portion of the thyroid cartilage; however, in horseshoe bats, the thyrohyoid muscle and caudal tip of the thyrohyal bone were connected to the lateral side and thyroid cranial cornua, respectively (Fig. 1A).

Larynx
Each anatomical module (cartilage, muscle, and nerve) is illustrated in Fig. 2. The cricoid cartilage had a sagittal crest in horseshoe bats, completely dividing the dorsal cricoarytenoid muscle into left and right components (Figs. 1A–C, 2A). The thyroid cartilage had the cranial and caudal cornua connected to the thyrohyal bone and muscular wings of the cricoid cartilage in bats. The rostroventral tip of the thyroid cartilage was separated to form a pair of protuberances, to which the thyroarytenoid muscle was attached (Fig. 1B). While the thyroid cartilage of mice had one pair of the foramen thyroideum at the lamina of the thyroid cartilage, through which the cranial laryngeal nerve passes, that of the thyroid cartilage was not opened in the rhinolophoids. The cricothyroid muscle surrounding the cranial arch of the cricoid cartilage was significantly enlarged in bats compared to that in mice. While the cricothyroid muscle was separated into left and right components in mice, those of horseshoe bats met at the median line, forming one large muscle complex.

Trachea
A pair of lateral and dorsal tracheal chambers were present in the ventral portion of the cranial arch of the cricoid cartilage (Figs. 1A–D, 2A–D). The lateral tracheal chamber was completely attached to the ventral side of the cricoid cartilage and the dorsal tracheal chamber. Both tracheal chambers had a pouch-shaped structure surrounded by the glottis and tracheal rings and had internal cavities connected to the respiratory tract. The ventral portion of the cricothyroid muscle was attached to the dorsal side of the lateral tracheal chamber, denoting that the contraction of the tracheal chamber was regulated by the common muscle to generate the biosonar pulse.
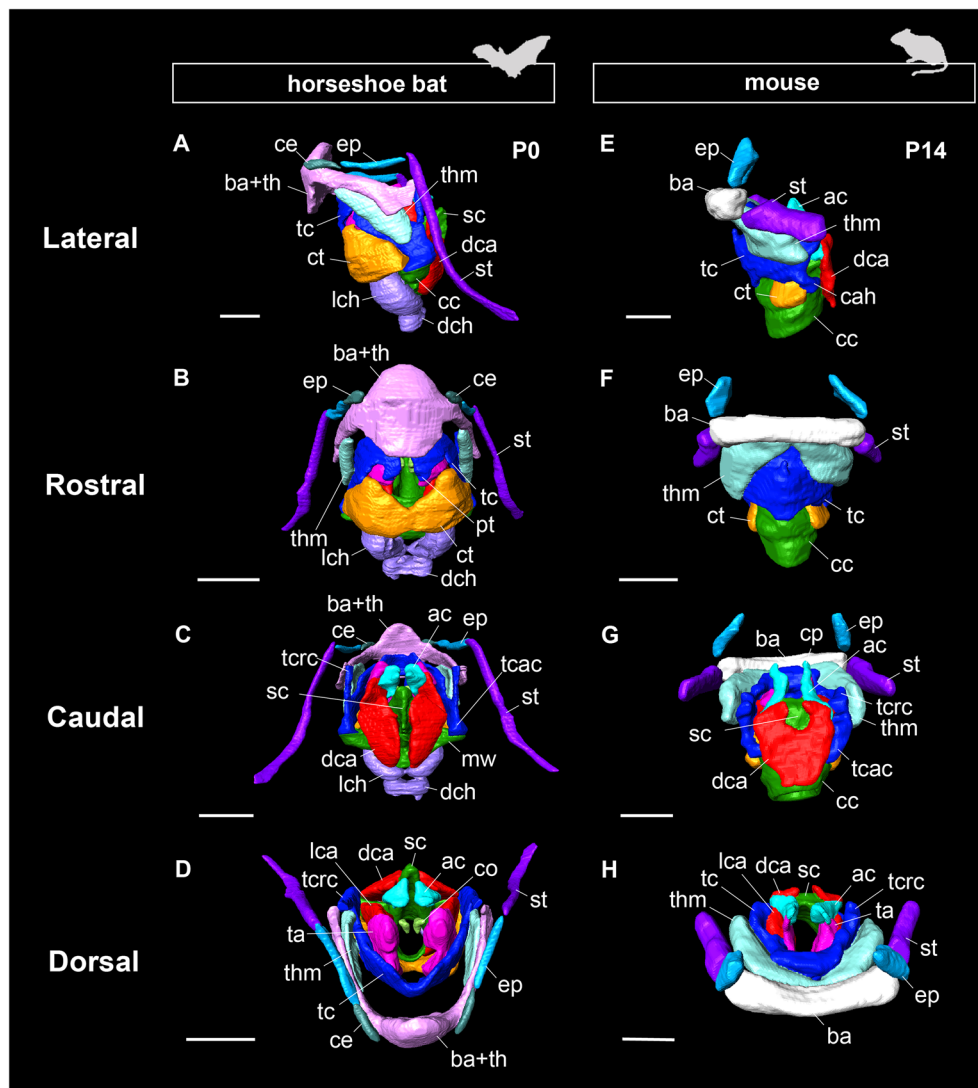
Fig. 1 The gross anatomy of the hyolaryngeal apparatus in bats (postnatal day 0 of *Rhinolophus pusillus*) and mice (postnatal day 14 of *Mus musculus*) reconstructed with the diffusible iodine-based contrast-enhanced CT scanning. Left side of the hyolaryngeal morphology is shown in lateral view. Scale bars = 1 mm. See text for abbreviations

Innervation

Figures 2 and 3 show the innervation pattern of the laryngeal muscles in CS22 of the horseshoe bat and E18.5 of the laboratory mouse, which were three-dimensionally reconstructed using immunohistochemical staining. The vagus nerve (cranial nerve X) had two branches, the cranial and recurrent laryngeal nerves. In mice, the cranial laryngeal nerve passed through the foramen thyroideum (Figs. 2E–H, 3E, F), whereas in bats, it passed below the thyroid cartilage and supplied the cricothyroid muscle (Figs. 2A–D, 3B). In the cricothyroid muscle of bats, the cranial laryngeal nerve had

two branches, rostral and ventral (Fig. 3D). These two branches passed through the rostral and ventral cricothyroid muscles, indicating that the ventral branch of the cranial laryngeal nerve supplied contractions to the lateral tracheal chamber. The recurrent laryngeal nerve, previously supplied in the postcranial direction, looped under the aortic arch, and reached the dorsal cricoarytenoid muscle in both bats and mice (Fig. 3D, H). The recurrent laryngeal nerve passed the dorsal cricoarytenoid muscle, was supplied to the lateral cricoarytenoid muscle, and finally to the thyroarytenoid muscle (Fig. 3C, G). The supply pattern of the recurrent laryngeal nerve was common between bats and mice.
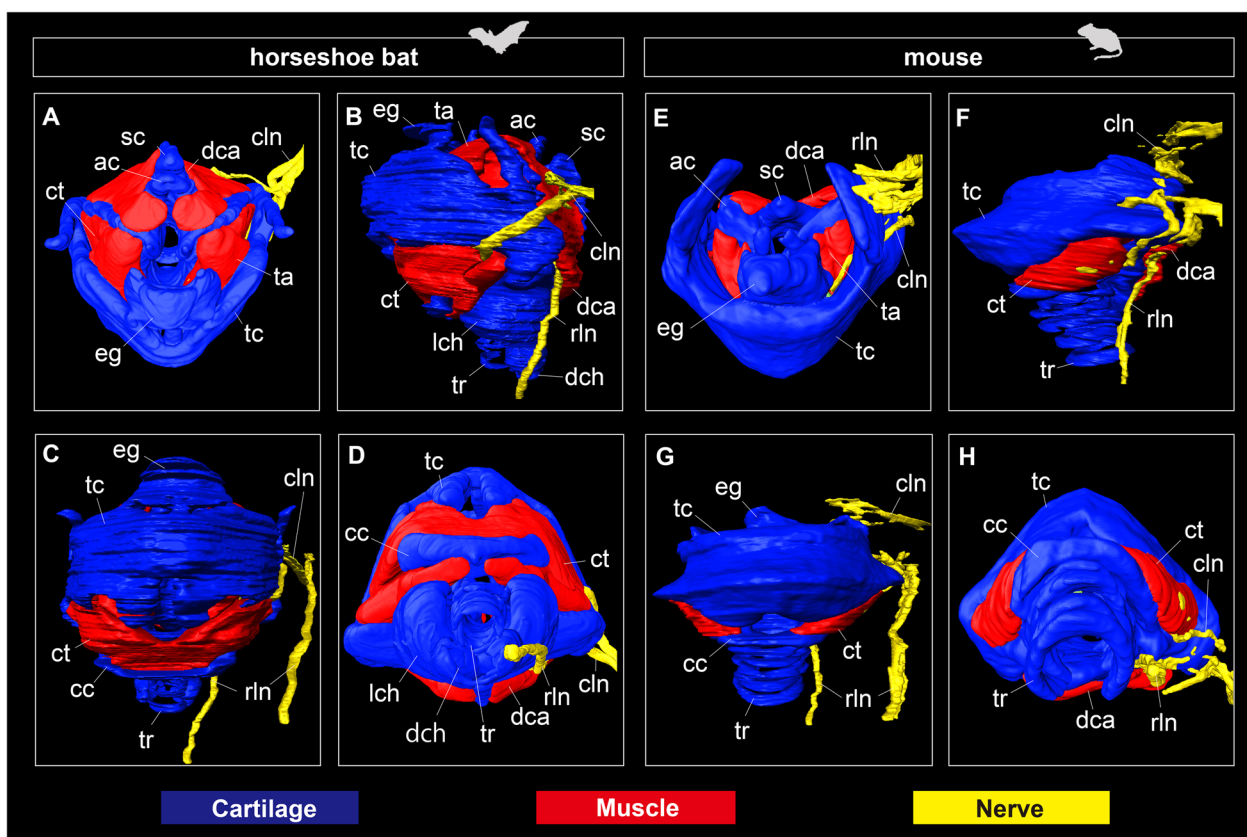
Fig. 2 The anatomical module of the larynx in CS22 individual of the horseshoe bat (*Rhinolophus malayanus*) and E18.5 individual of the laboratory mouse (*Mus musculus*). Green color refers to the cartilage: epiglottic cartilage, thyroid cartilage, cricoid cartilage, arytenoid cartilage, lateral and dorsal tracheal chamber, and tracheal rings. Red color refers to the muscle: cricothyroid muscle, dorsal and lateral cricoarytenoid muscle, and thyroarytenoid muscle. Blue color refers to the nerve: cranial and recurrent laryngeal nerve. **A** Dorsal view of the larynx of CS22 of *R. malayanus*. **B** Lateral view of the larynx of CS22 of *R. malayanus*. **C** Rostral view of the larynx of CS22 of *R. malayanus*. **D** Ventral view of the larynx of CS22 of *R. malayanus*. **E** Dorsal view of the larynx of E18.5 of *M. musculus*. **F** Lateral view of the larynx of E18.5 of *M. musculus*. **G** Rostral view of the larynx of E18.5 of *M. musculus*. **H** Ventral view of the larynx of E18.5 of *M. musculus*

Prenatal development of the hyolaryngeal complex in horseshoe bats and in mice

Hyoid development

Cartilaginous condensation began at mid-fetal stage (CS17) (Fig. 4A, B) in *Rhinolophus* bats. The cranial cornua, consisting of the ceratohyal, epihyal, and stylohyal, was separated from the hyoid body (basihyal) and caudal cornua (thyrohyal), but was not segmented to form each component. The thyrohyoid muscle, connecting the hyoid apparatus to the laryngeal cartilage, was present in the rostrolateral portion of the hyoid complex and thyroid cartilage.

The condensed hyoid chondrocytes differentiated into ceratohyal, epihyal, and stylohyal at late-fetal stage (CS20.5) (Fig. 4C, D). Periosteum was observed around the stylohyal bone, denoting that the ossification started at this stage. The general morphology of the hyoid cartilage and muscle did not change from CS20.5 onward (Fig. 4E, F).

In *Mus musculus*, the epihyal, basihyal, thyrohyal, stylohyal cartilages, and thyrohyoid muscles were already evident at day 14.5 (E14.5), but the boundaries in each hyoid component were not evident (Fig. 4G, H). A connection between the hyoid and larynx was also achieved at this stage, after which there was no drastic change in the overall morphology of the hyolaryngeal complex (Fig. 4K, L).

Laryngeal development

Chondrification of the cricoid, thyroid, and arytenoid began at mid-fetal stage (CS17) in horseshoe bats. The cranial arch was formed at the ventral margin of the cricoid cartilage that surrounds the glottis. The sagittal crest projected dorsally from the medial portion of the cricoid cartilage. The cranial cornua of the thyroid cartilage was dorsally projected to connect to the hyoid complex. The corniculate processes of the arytenoid cartilage were by now in contact with one another. The cricothyroid,
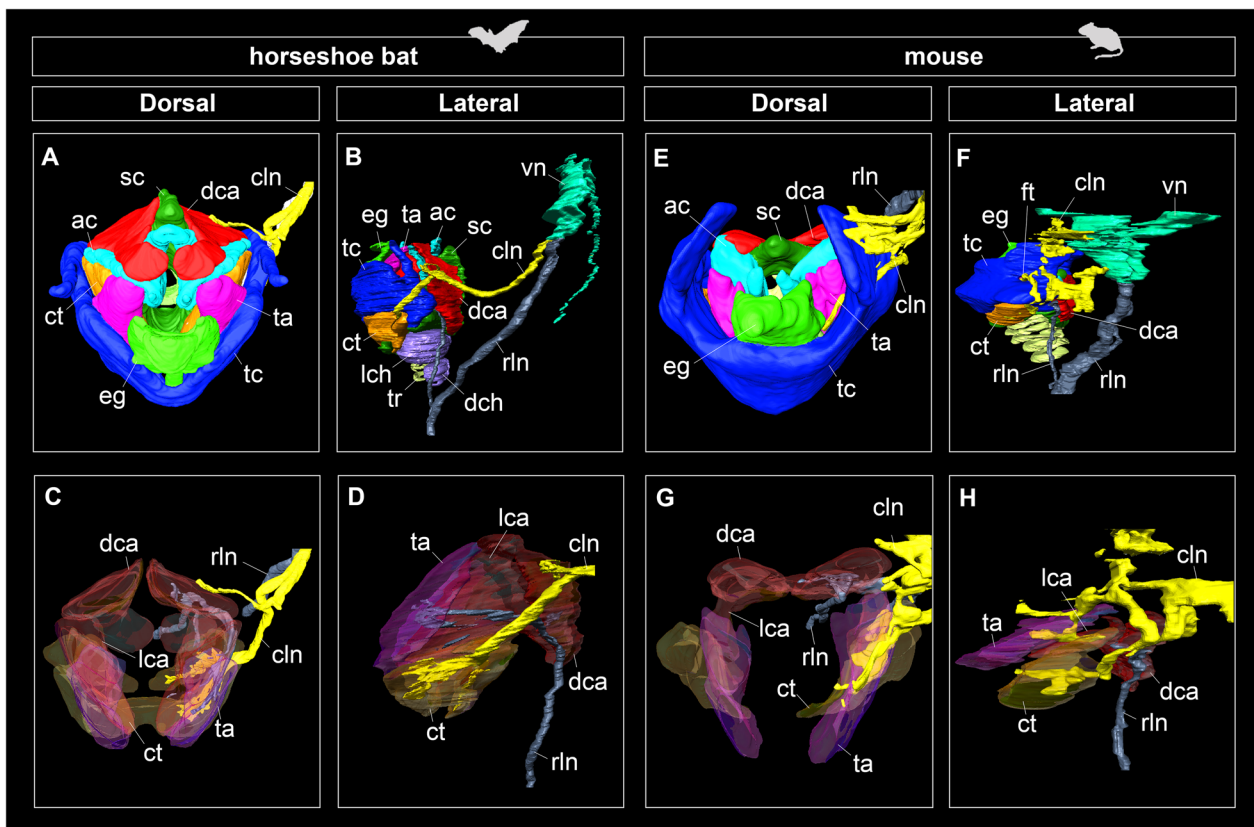
Fig. 3 The whole morphology of the intrinsic laryngeal muscle and innervations of the cranial laryngeal nerve and recurrent laryngeal nerve of CS22 stage in *Rhinolophus malayanus* and E18.5 stage in *Mus musculus*. **A** Dorsal view of the hyolaryngeal cartilages, intrinsic laryngeal muscles, and vagus nerve of CS22 fetus of *R. malayanus*. **B** Lateral view of the hyolaryngeal cartilages, intrinsic laryngeal muscles, and vagus nerve of CS 22 fetus of *R. malayanus*. **C** Dorsal view of the intrinsic laryngeal muscles and vagus nerve of CS22 fetus of *R. malayanus*. **D** Lateral view of the intrinsic laryngeal muscles and vagus nerve of CS22 fetus of *R. malayanus*. **E** Dorsal view of the hyolaryngeal cartilages, intrinsic laryngeal muscles, cranial laryngeal nerve, and recurrent laryngeal nerve of E18.5 fetus of *M. musculus*. **F** Lateral view of the hyolaryngeal cartilages, intrinsic laryngeal muscles, cranial laryngeal nerve, and recurrent laryngeal nerve of E18.5 fetus of *M. musculus*. **G** Dorsal view of the intrinsic laryngeal muscles, cranial laryngeal nerve, and recurrent laryngeal nerve of E18.5 fetus of *M. musculus*. **H** Lateral view of the intrinsic laryngeal muscles, cranial laryngeal nerve, and recurrent laryngeal nerve of E18.5 fetus of *M. musculus*. The cranial laryngeal nerve and recurrent laryngeal nerve were visualized using the immunohistochemistry of the acetylated tubulin antibody. The left side of the hyolaryngeal morphology is shown in lateral view. See text for abbreviations

cricoarytenoid, and thyroarytenoid muscles were present in CS17 (Fig. 5A–C). The cricothyroid muscle was formed at the rostroventral portion of the thyroid cartilage and the rostrodorsal portion of the cricoid cartilage, covering the cranial arch of the cricoid cartilage. The thyroarytenoid muscle was formed at the ventral part of the arytenoid cartilage, protruding toward the thyroid cartilage. The lateral and dorsal cricoarytenoid muscles were formed at the rostral portion of the arytenoid cartilage and the caudal surface of the cricoid cartilage, respectively. The dorsal cricoarytenoid muscle was separated into left and right components by the sagittal crest of the cricoid cartilage (Fig. 5C).

The muscular wings of the cricoid cartilage projected bilaterally to form a joint with the caudal cornua of the thyroid cartilage in late fetal stage (CS20.5) (Fig. 5E, F). The sagittal crest of the cricoid cartilage was projected to be greater than that of the CS17. The dorsal tip of the cranial cornua of the thyroid cartilage was slightly curved. In dorsal view, the rostral tip of the thyroid cartilage was curved, forming a V-shaped morphology (Fig. 5E). The vocal processes of the arytenoid cartilage were projected medially around the glottis. The muscular process of the arytenoid cartilage also projected bilaterally. The cricothyroid muscle further expanded toward the tracheal region to surround the cranial arch of the cricoid cartilage. The thyroarytenoid muscle extended rostrally and attached to thyroid cartilage. The dorsal cricoarytenoid muscle expanded dorsoventrally along the sagittal crest of cricoid cartilage.
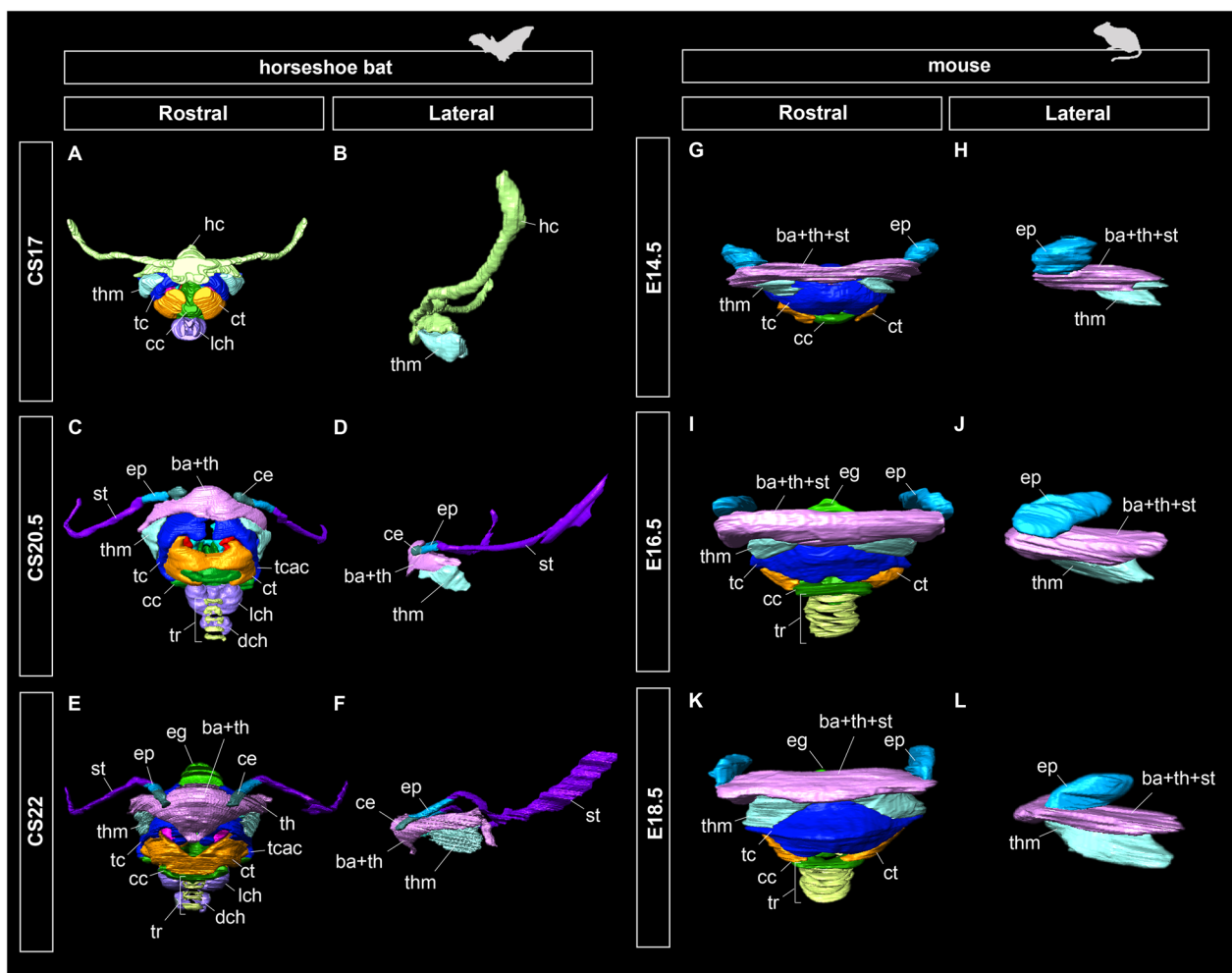
Fig. 4 Prenatal development of the hyoid apparatus in horseshoe bats (CS17, CS20.5, CS22) and *Mus musculus* (E14.5, E16.5, E18.5), three-dimensionally reconstructed using serial tissue sections. **A** Rostral view of the hyolaryngeal apparatus of CS17 fetus of the horseshoe bat. **B** Lateral view of the hyoid components of CS17 fetus of *Rhinolophus pusillus*. **C** Rostral view of the hyolaryngeal apparatus of CS20.5 fetus of *R. malayanus*. **D** Lateral view of the hyoid components of CS20.5 fetus of *R. malayanus*. **E** Rostral view of the hyolaryngeal apparatus of CS22 fetus of *R. malayanus*. **F** Lateral view of the hyoid components of CS22 fetus of *R. malayanus*. **G** Rostral view of the hyolaryngeal apparatus of E14.5 fetus of *M. musculus*. **H** Lateral view of the hyoid components of E14.5 fetus of *M. musculus*. **I** Rostral view of the hyolaryngeal apparatus of E16.5 fetus of *M. musculus*. **J** Lateral view of the hyoid components of E16.5 fetus of *M. musculus*. **K** Rostral view of the hyolaryngeal apparatus of E18.5 fetus of *M. musculus*. **L** Lateral view of the hyoid components of E18.5 fetus of *M. musculus*. The tracheal chambers and tracheal rings of the horseshoe bats start those chondrifications at CS17 and CS20.5, respectively. The left side of the hyolaryngeal morphology is shown in lateral view. See text for abbreviations

At later fetal stage (CS22), the caudal cornua of the thyroid cartilage and muscular wings of the cricoid cartilage projected in the ventral and bilateral directions, respectively. The projection of the front portion occurred in the rostrolateral portion of the cranial arch of the cricoid cartilage. The rostral tip of the thyroid cartilage became more convex than in the previous stage. The muscular processes of the arytenoid cartilage protruded bilaterally to expand the attachment area of the dorsal cricoarytenoid muscle. The cricothyroid muscle expanded medially and the cranial arch of the cricoid cartilage was fully covered. The lateral portion of the cricothyroid muscle extended beyond the front plate of the cricoid cartilage and reached the trachea. The thyroarytenoid muscle extended rostrolaterally to expand the area attached to the thyroid cartilage. The dorsal cricoarytenoid muscle extended dorsorostrally and was attached to the depression between the corniculate and the vocal processes of the arytenoid cartilage.

Similarly, in mice, the cricoid, thyroid, and arytenoid cartilages were already chondrified at E14.5 (Fig. 5J). The sagittal crest of the cricoid cartilage was slightly
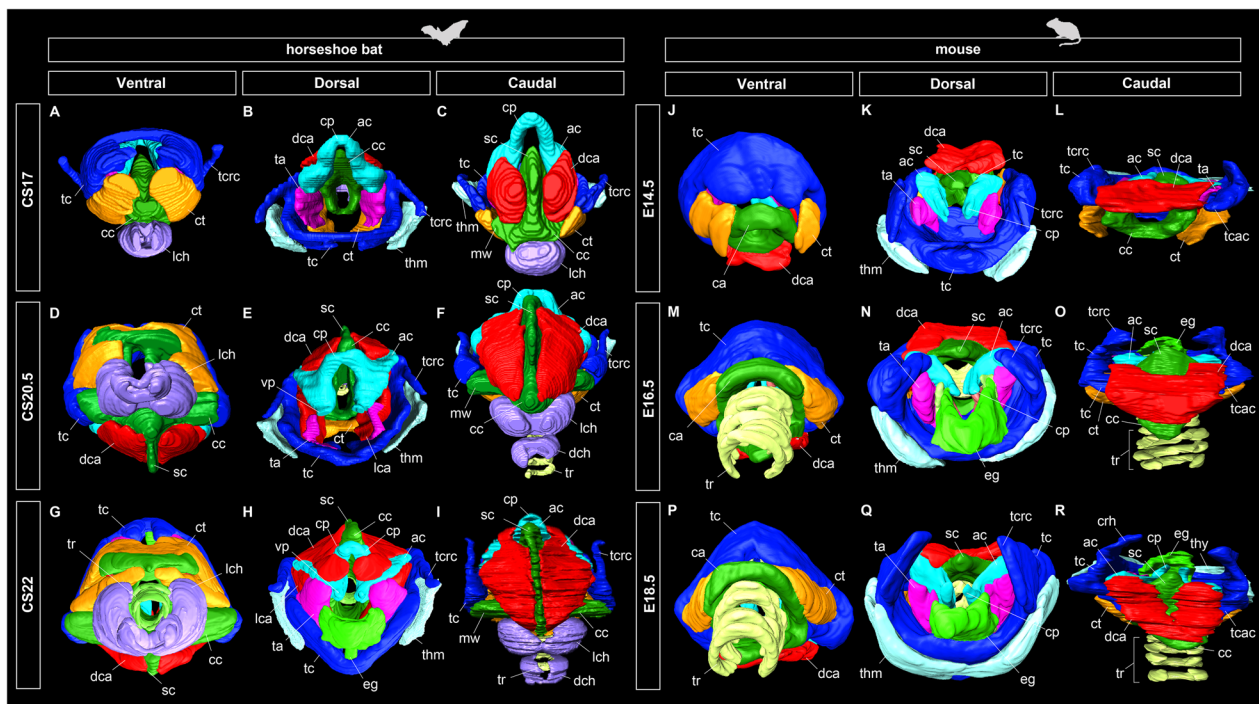
Fig. 5 Prenatal laryngeal development of horseshoe bats and laboratory mice, three-dimensionally reconstructed from serial tissue sections. See text for abbreviations. **A** Ventral view of the hyolaryngeal apparatus of CS17 fetus of *Rhinolophus pusillus*. **B** Dorsal view of the hyolaryngeal apparatus of CS17 fetus of *R. pusillus*. **C** Caudal view of the hyolaryngeal apparatus of CS17 fetus of *R. pusillus*. **D** Ventral view of the hyolaryngeal apparatus of CS20.5 fetus of *R. pusillus*. **E** Dorsal view of the hyolaryngeal apparatus of CS20.5 fetus of *R. malayanus*. **F** Caudal view of the hyolaryngeal apparatus of CS20.5 fetus of *R. malayanus*. **G** Ventral view of the hyolaryngeal apparatus of CS22 fetus of *R. pusillus*. **H** Dorsal view of the hyolaryngeal apparatus of CS22 fetus of *R. malayanus*. **I** Caudal view of the hyolaryngeal apparatus of CS22 fetus of *R. malayanus*. **J** Ventral view of the hyolaryngeal apparatus of E14.5 fetus of *Mus musculus*. **K** Dorsal view of the hyolaryngeal apparatus of E14.5 fetus of *M. musculus*. **L** Caudal view of the hyolaryngeal apparatus of E14.5 fetus of *M. musculus*. **M** Ventral view of the hyolaryngeal apparatus of E16.5 fetus of *M. musculus*. **N** Dorsal view of the hyolaryngeal apparatus of E16.5 fetus of *M. musculus*. **O** Caudal view of the hyolaryngeal apparatus of E16.5 fetus of *M. musculus*. **P** Ventral view of the hyolaryngeal apparatus of E18.5 fetus of *M. musculus*. **Q** Dorsal view of the hyolaryngeal apparatus of E18.5 fetus of *M. musculus*. **R** Caudal view of the hyolaryngeal apparatus of E18.5 fetus of *M. musculus*

projected. The cranial arch of the cricoid cartilage surrounding the glottis was evident. The thyroid cranial cornua projected dorsally to form a joint with the hyoid complex. The rostral tip of the thyroid cartilage was convex in the dorsal view. The arytenoid cartilage had already undergone a corniculate process. The cricothyroid muscle was also evident, running between the ventrocaudal and dorsorostral portions of the thyroid cartilage. The thyroarytenoid muscle was formed at the rostral site of the arytenoid cartilage and attached to the caudal side of the thyroid cartilage. The lateral cricoarytenoid muscle at the rostroventral site of the arytenoid cartilage remained small. The dorsal cricoarytenoid muscle was still not in contact with the lateral cricoarytenoid muscle and was not separated by the sagittal crest of the cricoid cartilage, similar to that in horseshoe bats (Fig. 5L). At E16.5, the cricoid cartilage expanded ventrally to expand the attachment area of the dorsal cricoarytenoid muscle. The thyroid cartilage was in contact with the muscular wings of the cricoid cartilage. In contrast to horseshoe bats, a

pair of the foramen thyroideum was opened at the lateral lamina of the thyroid cartilage, through which the cranial laryngeal nerve passes. From E16.5 onward, the morphology of the laryngeal cartilage did not change drastically (Fig. 5M–O). At E18.5, the dorsal cricoarytenoid muscle was separated by the caudally projected sagittal crest of the cricoid cartilage but was not fully divided, as in bats (Fig. 5P–R). As for the cricothyroid muscle, the rostral tips of the left and right muscles did not meet or reach the trachea; thus, the cranial arch of the cricoid cartilage remained exposed, unlike in horseshoe bats.

Tracheal development
In horseshoe bats, chondrification of the tracheal ring was not evident at mid-fetal stage (CS17), whereas chondrocytes were condensed in the region of the lateral tracheal chamber, denoting that the lateral tracheal chamber is a novel laryngeal cartilage acquired in horseshoe bats (Fig. 6A). Condensed chondrocytes in the lateral tracheal chamber were continuous with

those in the cricoid cartilage (Fig. 6A-2). At late-fetal stage (CS22), the tracheal rings began to chondrify (Fig. 6B). Simultaneously, the dorsal tracheal chamber was chondrified ventrally into the lateral tracheal chamber. The condensed chondrocytes in both the lateral and dorsal tracheal chambers were separated to form the left and right tracheal chambers (Fig. 6B-2, B-3). The lateral tracheal chamber covered the tracheal region from the cranial arch of the cricoid cartilage to the third tracheal ring, while the dorsal tracheal chamber covered the fourth to sixth tracheal rings. The lateral tracheal chamber was articulated with the cranial arch of the cricoid cartilage (Fig. 6B-2), whereas the dorsal tracheal chamber was connected to the sixth tracheal ring (Fig. 6B-4). The ventral portion of the cricothyroid muscle reached the caudal side of a pair of lateral tracheal chambers.

In laboratory mice, tracheal rings were not evident at E14.5 with all components of the laryngeal cartilage (Fig. 6C). Tracheal rings were chondrified ventrally to the cranial arch of the cricoid cartilage at E16.5 (Fig. 6D), after which there was no drastic shift in the morphology of the tracheal region (Fig. 6E).

Pre- and postnatal ossification and mineralization of the hyolaryngeal apparatus

The presence of ossification of all craniocervical bony elements at each stage is summarized in Additional file 1: Tables S1–3. In horseshoe bats, ossification of the stylohyal occurred at mid-fetal stage (CS19) and other hyoid components did not start until late-fetal stage (CS21) (Fig. 7). The epihyal and thyrohyal were simultaneously ossified in the rostral region of the stylohyal in the CS22. In E18.5mice, the basihyal and ceratohyal regions ossified
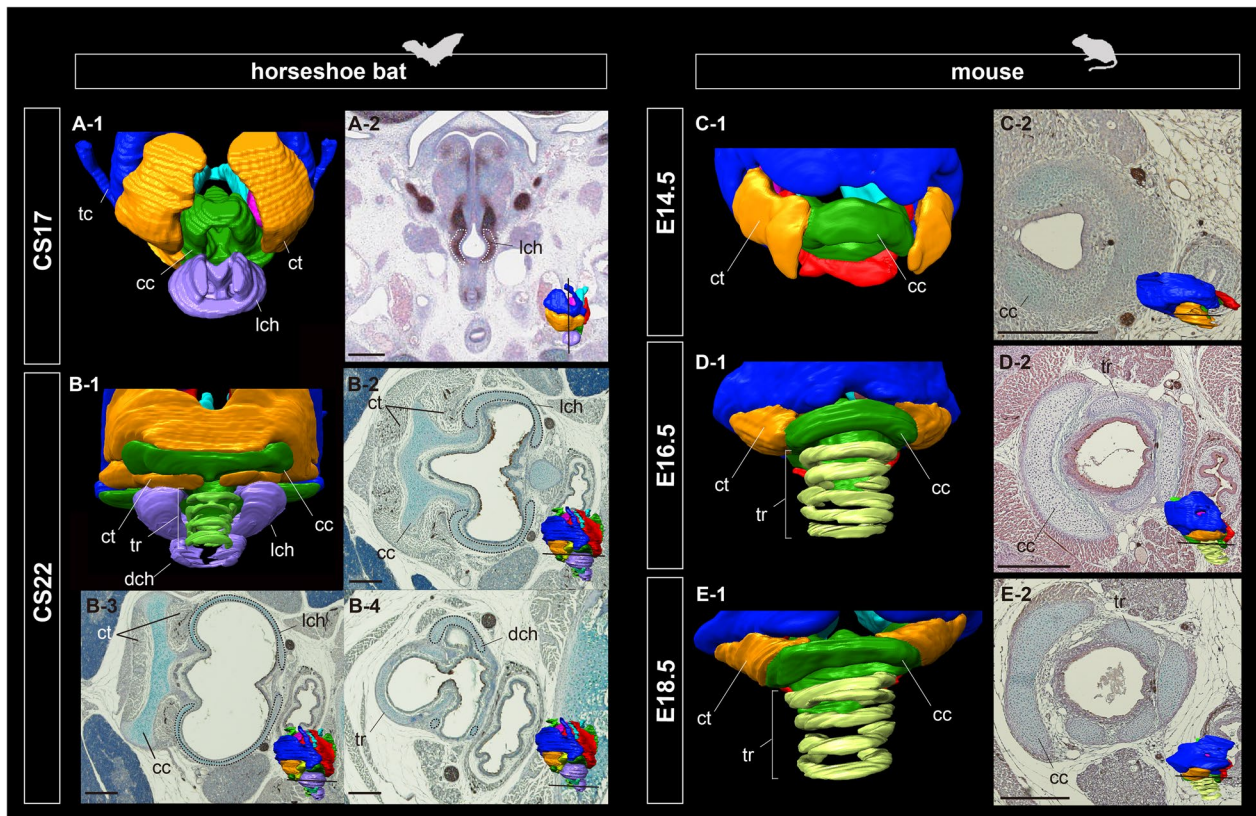

Fig. 6 The three-dimensional reconstruction of the fetal tracheal development and histological observations in horseshoe bats and laboratory mice using immunohistochemistry. **A-1** The tracheal anatomy of CS17 fetal specimen of *Rhinolophus pusillus*. **A-2** The histological section of the hyolarynx of CS17 fetal specimen of *R. pusillus*, stained by hematoxylin and immunohistochemistry of Sox9. **B-1** The tracheal anatomy of CS22 fetal specimen of *R. malayanus*. **B-2** to **B-4** The histological sections of the hyolarynx of CS22 fetal specimen of *R. malayanus*, stained by alcian blue, hematoxylin, and immunohistochemistry of acetylated tubulin antibody. **C-1** The tracheal anatomy of E14.5 fetal specimen of *Mus musculus*. **C-2** The histological section of the hyolarynx of E14.5 fetal specimen of *M. musculus*, stained by alcian blue, hematoxylin, and immunohistochemistry of acetylated tubulin antibody. **D-1** The tracheal anatomy of E16.5 fetal specimen of *M. musculus*. **D-2** the histological section of the hyolarynx of E16.5 fetal specimen of *M. musculus*, stained by alcian blue, hematoxylin, and immunohistochemistry of acetylated tubulin antibody. **E-1** The tracheal anatomy of E18.5 fetal specimen of *M. musculus*. **E-2** The histological section of the hyolarynx of E18.5 fetal specimen of *M. musculus*, stained by alcian blue, hematoxylin, and immunohistochemistry of acetylated tubulin antibody. Scale bars = 500 μm. See text for abbreviations

between the left and right thyrohyal and rostral regions of the epihyal region, respectively. Simultaneously, mineralization of the laryngeal cartilaginous elements, cricoid, thyroid, and arytenoid, became evident. The center of mineralization of the cricoid cartilage was observed in the proximal part of the cranial arch. The mineralization
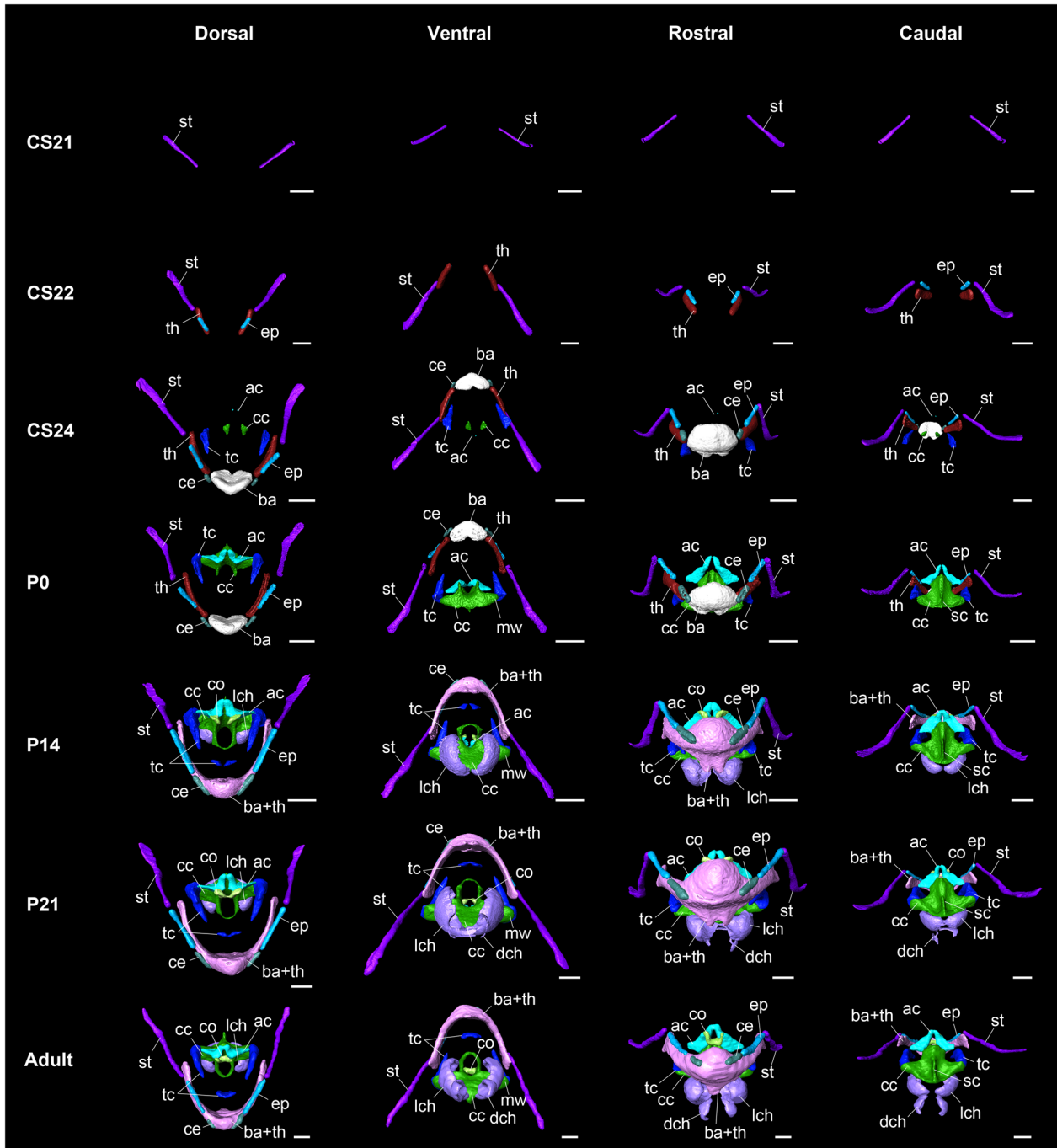
Fig. 7 Three-dimensional reconstruction of the pre- and postnatal ossification and mineralization of the hyolaryngeal apparatus in horseshoe bats. Scale bars = 1 mm. See text for abbreviations. CS21: fetal specimen of *Rhinolophus pusillus*. The stylohyal is ossified. CS22: fetal specimen of *R. pusillus*. The thyrohyal and epihyal are ossified. CS24: fetal specimen of *R. pusillus*. The basihyal and thyrohyal are ossified. The arytenoid, cricoid, and thyroid cartilages are mineralized. P0: postnatal day 0 specimen of *R. pusillus*. The sagittal crest of the cricoid cartilage is mineralized. P14: postnatal day 14 specimen of *R. pusillus*. The lateral tracheal chambers are mineralized. P21: postnatal day 21 specimen of *R. pusillus*. The dorsal tracheal chambers are mineralized. Adult: adult specimen of *R. pusillus*

of the thyroid cartilage starts from the lateral part, at which point the future joint with the cricoid cartilage is formed. Mineralization of the arytenoid cartilage begins at the caudal tip of the corniculate process. In postnatal day 0 (P0) specimens of horseshoe bats, the mineralized cricoid cartilage further expanded to form muscular wings and a cricoid lamina with the sagittal crest. The proximal part of the cranial arch extended rostrally. The muscular wings of the cricoid cartilage were in contact with those of the thyroid cartilage. The small ossification center of the arytenoid cartilage in CS24 expanded to form corniculate and muscular processes immediately after birth. At P14, the stylohyal, epihyal, ceratohyal, and thyrohyal regions extend caudally. The thyrohyal and basihyal were fully fused and the suture was absent. The sagittal crest of the cricoid cartilage extended caudally. The cranial arch of the cricoid cartilage was further mineralized to fully cover the glottis. A pair of cranial cornua of the thyroid cartilage was mineralized caudally to the basihyal. The vocal process projected slightly at the ventral base of the arytenoid cartilage. The left and right dorsal tips of the corniculate processes were in contact with each other. From this stage onward, mineralization of the lateral tracheal chamber began. The lateral tracheal chamber was in contact with the ventral side of the cricoid cartilage, forming an internal cavity connected to the respiratory tract. The sagittal crest of the cricoid cartilage extended dorsally at P21. The left and right mineralized cranial cornua of the thyroid cartilage were merged. The left and right vocal processes of the arytenoid cartilage were also in contact with the median line. From P21 onward, the dorsal tracheal chamber began to mineralize. The mineralized portion of the dorsal tracheal chamber was in contact with the ventral portion of the lateral tracheal chamber. In adult horseshoe bats, the sagittal crest of the cricoid cartilage was sharper and thicker than that in juveniles. The mineralized lateral and dorsal tracheal chambers also thickened until sexual maturation.

Figure 7 shows the comparative anatomy of postnatal hyoid ossification and laryngeal mineralization in bats and mice. The relative ossification timing of the hyoid components is shown in Fig. 8 and Additional file 1: Table S3. While only the basihyal was ossified in P0 mice, all components of the hyoid apparatus started their ossification just after birth in bats. Indeed, except for the basihyal, almost all components of the hyoid apparatus ossified at an earlier stage in bats than in mice. Laryngeal mineralization was limited to the cricoid and thyroid cartilages in mice, whereas in bats, three laryngeal cartilages—the cricoid, thyroid, and arytenoid cartilages—were mineralized. Mineralization of the thyroid cartilage occurred in almost all parts of the mice, whereas in bats,
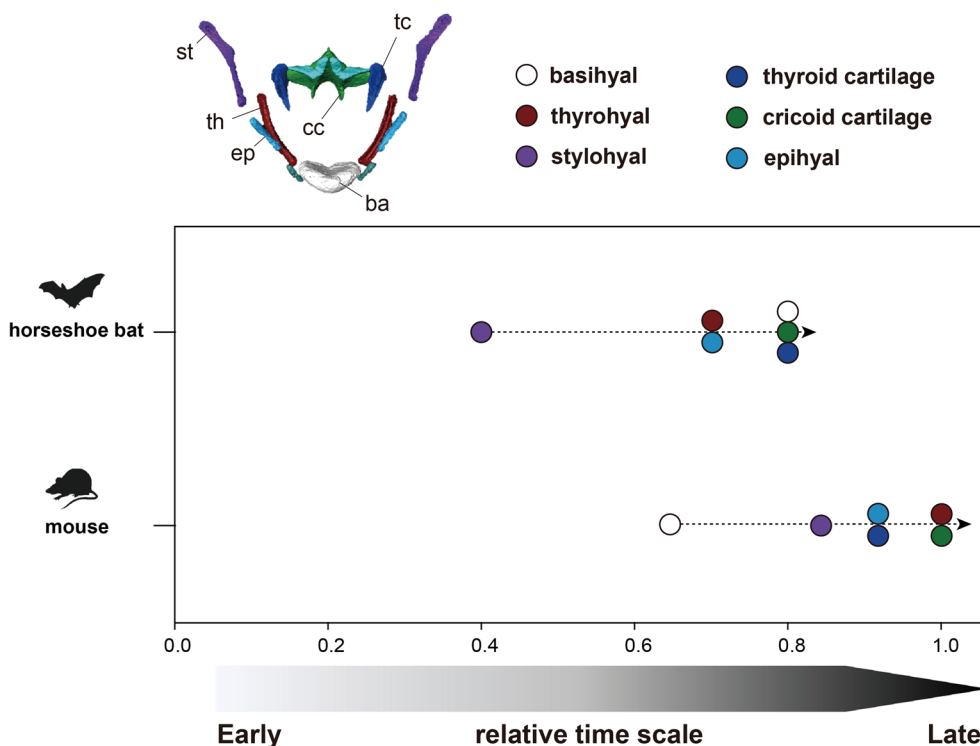

Fig. 8 The relative ossification and mineralization timing of the bony and cartilaginous components of the hyolaryngeal apparatus in horseshoe bats (red) and laboratory mice (white). See text for abbreviations

the mineralized area of the thyroid cartilage was partial (Fig. 9A–F). Regarding the mineralization rate, laryngeal mineralization occurred in a relatively short period (P14-adult), while that of bats proceeded over the long term (CS24-adult).

Allometric growth of the larynx and echolocation pulse ontogeny

The basic statistics and results of the reduced major axis (RMA) regression analyses of mineralized laryngeal cartilage against the cubed geometric mean (GM^3) of skull size in horseshoe bats are shown in Table 1 and Fig. 10A–D. A significant correlation with $\log_{10}$-transformed GM^3

was detected in all log10-transformed volumes of mineralized laryngeal cartilage: cricoid cartilage ($r = 0.90$, $p < 0.001$), thyroid cartilage ($r = 0.88$, $p < 0.001$), arytenoid cartilage ($r = 0.93$, $p < 0.001$), and lateral tracheal chamber ($r = 0.88$, $p < 0.001$). The allometric exponents of all laryngeal cartilages were above 1.0 (i.e. positive allometry) as follows: 2.01 in the cricoid cartilage (95% CI from 1.21 to 2.83), 3.20 in the thyroid cartilage (95% CI from 1.82 to 4.39), 3.93 in the arytenoid cartilage (95% CI from 2.72 to 4.88), and 5.66 in the lateral tracheal chamber (95% CI from 3.14 to 7.69). The y-intercept values were -5.68 in the cricoid (95% CI from -7.95 to -3.43), -9.46 in the thyroid (95% CI from -12.82 to -5.59), -11.68 in the
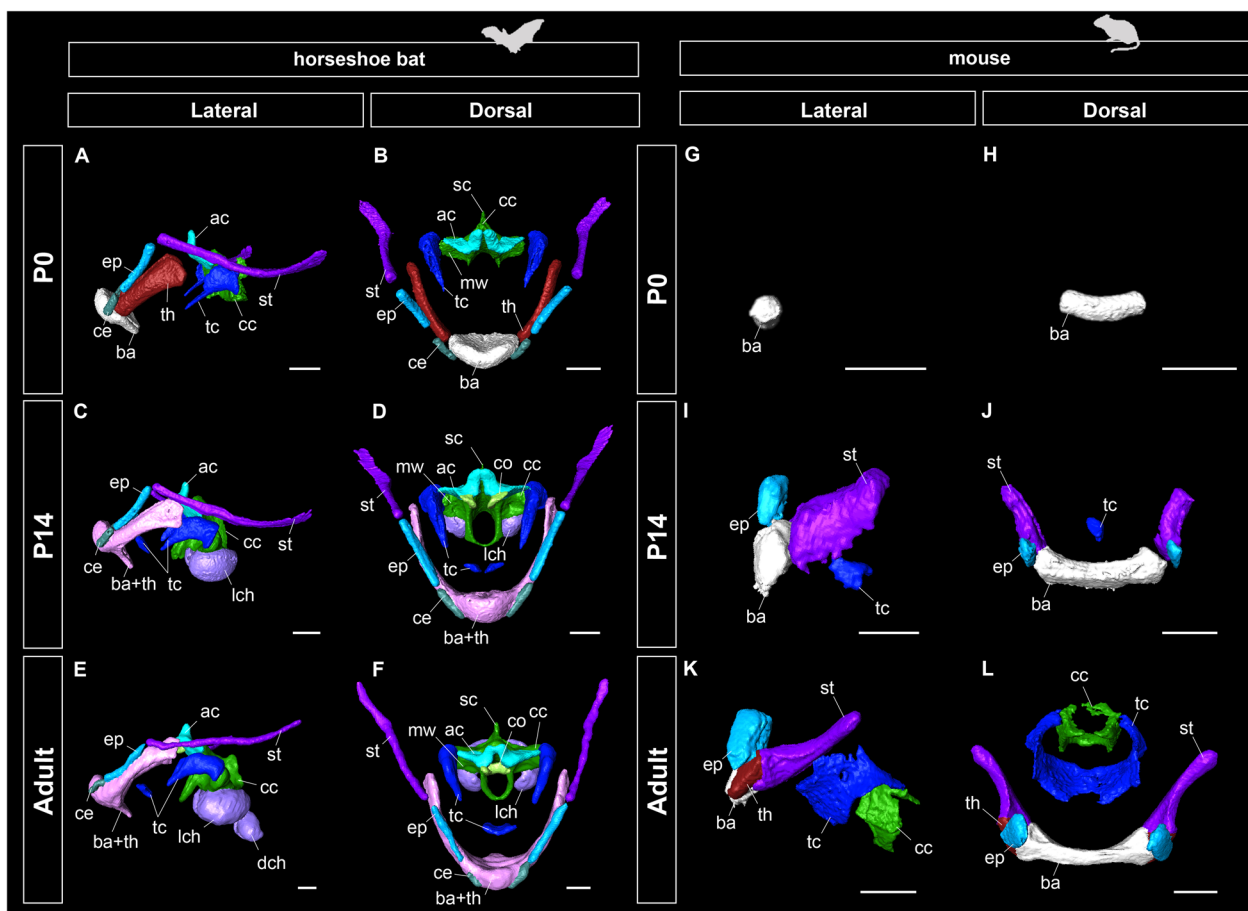

Fig. 9 Three-dimensional reconstruction of postnatal ossification and mineralization of the hyolaryngeal apparatus in horseshoe bats (*Rhinolophus pusillus*) and laboratory mice (*Mus musculus*) based on micro-CT scanning. Scale bars = 1 mm. See text for abbreviations. **A** Lateral view of the hyolaryngeal apparatus of the postnatal day 0 specimen of *R. pusillus*. **B** Dorsal view of the hyolaryngeal apparatus of the postnatal day 0 specimen of *R. pusillus*. **C** Lateral view of the hyolaryngeal apparatus of the postnatal day 14 specimen of *R. pusillus*. **D** Dorsal view of the hyolaryngeal apparatus of the postnatal day 14 specimen of *R. pusillus*. **E** Lateral view of the hyolaryngeal apparatus of the adult specimen of *R. pusillus*. **F** Dorsal view of the hyolaryngeal apparatus of the adult specimen of *R. pusillus*. **G** Lateral view of the hyolaryngeal apparatus of the postnatal day 0 specimen of *M. musculus*. **H** Dorsal view of the hyolaryngeal apparatus of the postnatal day 0 specimen of *M. musculus*. **I** Lateral view of the hyolaryngeal apparatus of the postnatal day 14 specimen of *M. musculus*. **J** Dorsal view of the hyolaryngeal apparatus of the postnatal day 14 specimen of *M. musculus*. **K** Lateral view of the hyolaryngeal apparatus of the adult specimen of *M. musculus*. **L** Dorsal view of the hyolaryngeal apparatus of the adult specimen of *M. musculus*

Table 1 Basic statistics of the allometric analyses of log10-transformed volume of the mineralized laryngeal cartilages or echolocation pulse, against log10-transformed geometric mean (GM)

	Slope (95%CI)	Intercept (95% CI)	*r*	*p*-value
Cricoid cartilage	2.01 (1.21~2.83)	−5.68 (−7.95~−3.43)	0.90	*p* < 0.0001
Thyroid cartilage	3.20 (1.82~4.39)	−9.46 (−12.82~−5.59)	0.88	*p* < 0.001
Arytenoid cartilage	3.93 (2.71~4.88)	−11.68 (−14.36~−8.23)	0.93	*p* < 0.001
Tracheal chamber	5.66 (3.14~7.69)	−16.47 (−22.21~−9.36)	0.88	*p* < 0.01
CF1	0.47 (0.04~0.73)	0.39 (−0.36~1.61)	0.76	0.0165
CF2	0.46 (0.05~0.73)	0.70 (−0.04~1.88)	0.76	0.0166
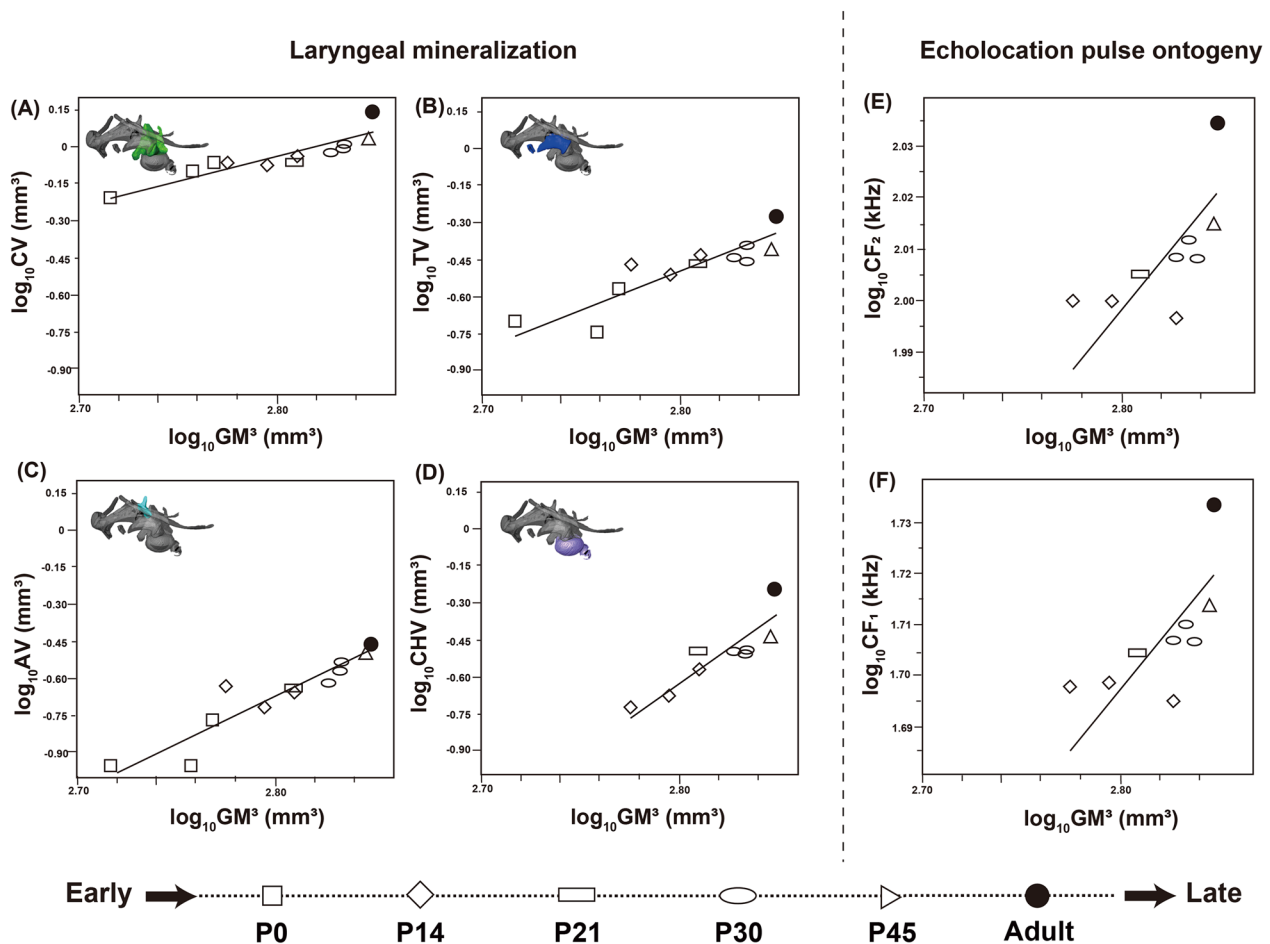
Fig. 10 The regression analyses based on the reduced major axis between the mineralized volume of the laryngeal cartilages or pulse peak frequency against skull size (cubed geometric mean). **A** $\log_{10}$-transformed volume of the mineralized cricoid cartilage and $\log_{10}$-transformed GM^3; **B** $\log_{10}$-transformed volume of the mineralized thyroid cartilage and $\log_{10}$-transformed GM^3; **C** $\log_{10}$-transformed volume of the mineralized arytenoid cartilage and $\log_{10}$-transformed GM^3; **D** $\log_{10}$-transformed volume of the mineralized tracheal chamber and $\log_{10}$-transformed GM^3; **E** $\log_{10}$-transformed CF_2 peak frequency and $\log_{10}$-transformed GM; **F** $\log_{10}$-transformed CF_1 peak frequency and $\log_{10}$-transformed GM^3. CV: cricoid cartilage volume; TV: thyroid cartilage volume; AV: arytenoid cartilage volume; CHV: tracheal chambers volume; GM^3: cubed geometric mean of the skull height (SH), skull length (SL), and skull width (SW). Note that plots for P0 individuals are not shown in **D**, **E**, and **F**, as mineralization and echolocation pulse are absent at this stage

arytenoid (95% CI from -14.36 to -8.23), and -16.47 in the lateral tracheal chamber (95% CI from -22.21 to -9.36).

The results of the RMA regression analyses of the log10-transformed maximum frequency of the first-harmonic (CF_1) and second-harmonic (CF_2) pulses against the log10-transformed GM^3 are shown in Fig. 10E–F. Significant correlations with the GM were detected for CF_1 ($r=0.76$, $p<0.05$) and CF_2 ($r=0.76$, $p<0.05$). The regression slope of both CF_1 and CF_2 significantly shows negative allometry as follows: 0.47 in CF_1 (95% CI from 0.04 to 0.73) and 0.46 in CF_2 (95% CI from 0.05 to 0.73). The y-intercept value was 0.39 in the CF_1 (95% CI from -0.36 to 1.61) and 0.70 in the CF_2 (95% CI from -0.04 to 1.88).

Figure 10 shows the ontogeny of the sonograms of the CF_1 and CF_2 pulses. The echolocation pulse was not confirmed until P13; thus, the biosonar pulse emission was acquired for at least 2 weeks after birth. At P14, the maximum frequencies of CF_1 and CF_2 were 49.58–49.99 kHz and 99.20–99.98 kHz, respectively. The values of CF_1 and CF_2 in P21 were 50.67 kHz and 101.23 kHz, respectively. In P30, the obtained values of each harmonic pulse were 50.89–51.28 kHz and 101.83–102.67 kHz. The maximum value of each harmonic pulse rose to 51.69 kHz and 103.37 kHz in P45. In adult individuals, the maximum frequencies of CF_1 and CF_2 finally reached 54.14 kHz and 108.25 kHz.

Relationship between laryngeal mineralization and pulse ontogeny

Table 2 and Fig. 11 illustrate the results of generalized linear model (GLM) analyses in horseshoe bats to investigate the relationship between the log10-transformed volume of the mineralized laryngeal cartilage and the log10-transformed peak frequencies of the CF_1 and CF_2 components of the echolocation pulse.

Significant positive associations with the maximum frequency of the CF_1 component were observed in the cricoid (slope=0.21, standard error [SE]=0.04, $p<0.001$), thyroid (slope=0.15, SE=0.06, $p<0.001$), arytenoid (slope=0.15, SE=0.04, $p<0.001$), and lateral tracheal chambers (slope=0.09, SE=0.02, $p<0.001$). Regarding the associations with the maximum frequency of the CF_2 component, significant positive associations were detected in the cricoid cartilage (slope=0.21, SE=0.04, $p<0.001$), thyroid cartilage (slope=0.15, SE=0.06, $p<0.001$), arytenoid cartilage (slope=0.15, SE=0.04, $p<0.001$), and lateral tracheal chamber (slope=0.08, SE=0.02, $p<0.001$).

Discussion
General morphology of the hyolaryngeal complex in the horseshoe bats

The hyolaryngeal morphology of horseshoe bats has the following six unique characteristics compared to that of mice: (1) a spatial gap between the hyoid complex and thyroid cartilage; (2) enlarged intrinsic muscles (cricothyroid, thyroarytenoid, dorsal, and lateral cricoarytenoid muscles); (3) sagittal crest of the cricoid cartilage; (4) a fully separated dorsal cricoarytenoid muscle; (5) the presence of lateral and dorsal tracheal chambers, and (6) the additional branch of the cranial laryngeal nerve innervating the cricothyroid muscle. Characteristics (2), (3), and (5) are consistent with the descriptions of *Rhinolophus hipposideros* [44] and *Hipposideros caffer* [26]. As reported in other laryngeally echolocating bats [19, 50], the intrinsic laryngeal muscles of horseshoe bats are hypertrophied compared to those of mice, and the laryngeal cartilage is drastically modified to provide attachment sites for these muscles. The overall pattern of innervation of the intrinsic laryngeal muscles of horseshoe bats was identical to that of mice, except for a novel

Table 2 Basic statistics of the generalized linear model analyses between log10-transformed volume of the mineralized laryngeal cartilages and log10-transformed peak frequency of CF_1 or CF_2

| Laryngeal cartilage	Slope	Standard error of slope	Intercept	Standard error of intercept	*p*-value
CF1					
Cricoid cartilage	0.21	0.04	2.31	0.12	$p<0.0001$
Thyroid cartilage	0.15	0.06	2.21	0.19	$p<0.01$
Arytenoid cartilage	0.15	0.04	2.22	0.14	$p<0.001$
Lateral tracheal chamber	0.09	0.02	1.99	0.06	$p<0.0001$
CF2					
Cricoid cartilage	0.21	0.04	2.61	0.12	$p<0.0001$
Thyroid cartilage	0.15	0.06	2.51	0.18	$p<0.01$
Arytenoid cartilage	0.15	0.04	2.53	0.13	$p<0.0001$
Lateral tracheal chamber	0.08	0.02	2.29	0.06	$p<0.0001$
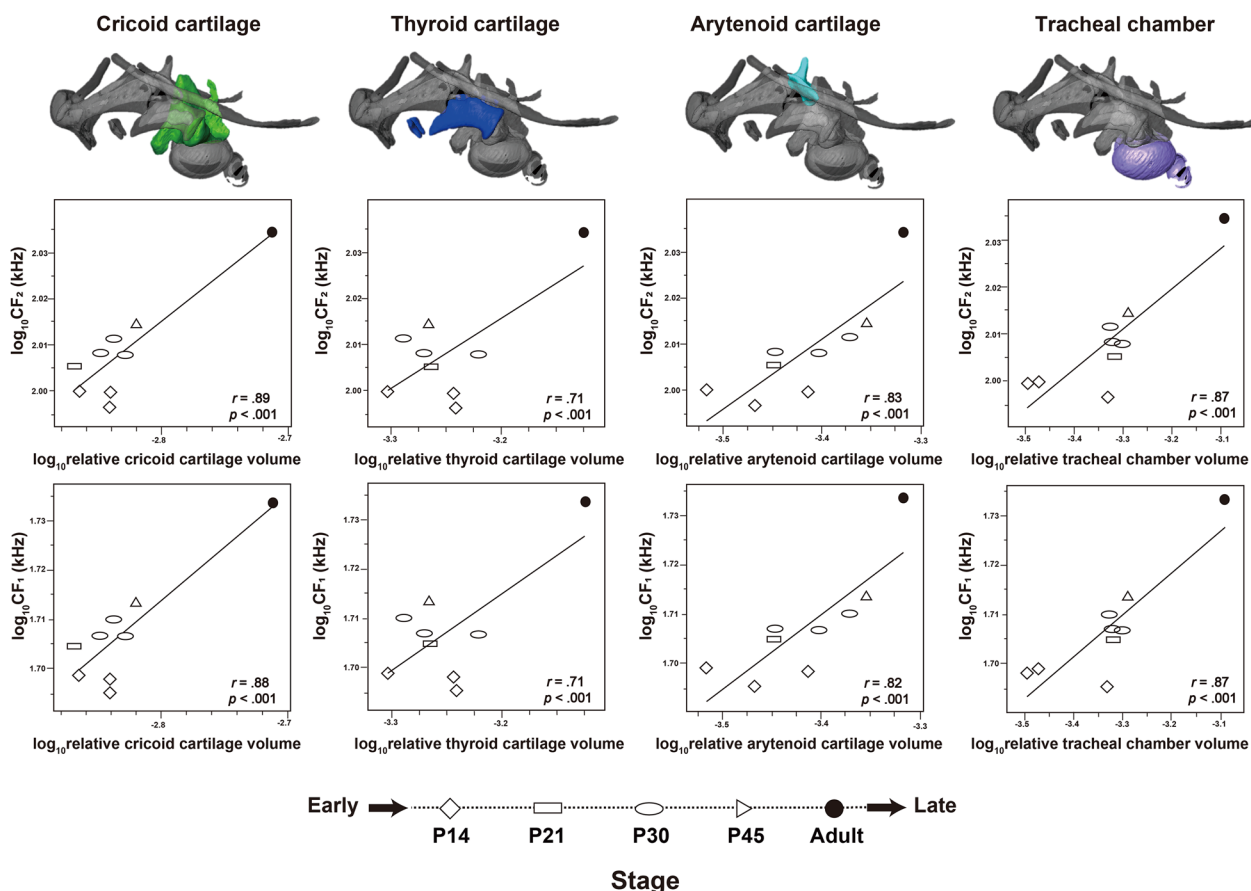
Fig. 11 GLM analyses between the pulse peak frequency and relative volume of the mineralized laryngeal cartilages. Each volume was normalized by the cubed geometric mean of the skull height (SH), skull length (SL), and skull width (SW)

branch of the cranial laryngeal nerve and the absence of the foramen thyroideum (Fig. 3).

Our observations identified a hyoid–larynx gap, showing that the connection between the hyoid and larynx is evident in horseshoe bats (Fig. 1D). This structure has also been confirmed in other laryngeally echolocating bats such as *Desmodus rotundus* [34] and *Artibeus jamaicensis* [48]. Instead, the stylohyal bone is articulated with the ectotympanic bone, which contributes to the direct conduction of ongoing echolocation signals in laryngeally echolocating bats [34] and tree mice [16]. However, these gaps and articulations are absent in pteropodids (Giannini et al. [60]) and non-bat mammals (Fig. 1G). Therefore, in laryngeally echolocating bats, the hyoid apparatus itself is likely to be extended rostrocaudally, providing a gap between the hyoid apparatus and laryngeal cartilage and articulation between the stylohyal and ectotympanic. Biosonar sound requires rotation of the thyroid cartilage to increase the tension of the vocal folds with the superfast muscle [19]. Acoustic response analyses have revealed that the bony connection between

the stylohyal and ectotympanic transfers sound signals at the most susceptible amplitude to the auditory bullae [40, 49]. Thus, as a result of the release from the tight connection, the hyoid complex and laryngeal cartilage might become mutually movable, providing higher flexibility for bone conduction and thyroid rotation, respectively.

The dorsal cricoarytenoid muscle was completely divided by the projection of the sagittal crest of the cricoid cartilage (Fig. 1C). In mice, the dorsal cricoarytenoid muscle was attached to the cricoid and arytenoid cartilages as a single muscle (Fig. 1G), whereas in bats, the separated left and right muscles were attached to the left and right arytenoid cartilages (Fig. 1C). This indicates that the separated dorsal cricoarytenoid muscle contracts independently, contributing to frequency adjustment in horseshoe bats. Generally, the dorsal cricoarytenoid muscle adducts with the arytenoid cartilage and adjusts the tension of the vocal folds during vocalization in mammals [57]. High-duty cycle (HDC) echolocating bats such as horseshoe bats emit sound signals multiple times per echolocation [22]. Previous studies have reported that

the sagittal crest of the cricoid cartilage is also protruding in laryngeally echolocating lineages that emit calls orally (Mormoopidae [58] and Vespertilionidae [46, 59]), whereas that of the non-laryngeally echolocating bats, the pteropodids, is relatively smooth [60]. In contrast to rhinolophids (this study) and hipposiderids [26], the sagittal crests of the cricoid cartilages in these groups do not fully divide the dorsal cricoarytenoid muscles, indicating that this muscle pattern is unique to HDC-echolocating rhinolophoids. Therefore, the independent contraction of the dorsal cricoarytenoid muscle caused by the development of the sagittal crest of the cricoid cartilage would increase the abduction ficiency of the arytenoid cartilage during HDC pulse emission in horseshoe bats.

We confirmed that the cricothyroid muscle, possibly innervated by a novel branch of the cranial laryngeal nerve, had expanded toward the lateral tracheal chamber (Fig. 3). The lateral and dorsal tracheal chambers have been hypothesized to be key features involved in pulse emission through the nostrils in the genera *Rhinolophus* and *Hipposideros* in rhinolophoids and nycterids [26, 44]. Tracheal chambers have been theorized to function as Helmholtz resonators that increase sound intensity for laryngeal echolocation [26, 29]. Because biosonar pulse generation is underpinned by the superfast contraction of the cricothyroid muscle in laryngeally echolocating bats (Elemans et al. [19]), the expansion and contraction of the tracheal chambers are likely synchronized with that of the cricothyroid muscle. If the hypertrophied cricothyroid muscle and additional branches of the cranial laryngeal nerve are required for acoustic function in the tracheal chambers, this innervation pattern would be a synapomorphy of rhinolophid and hipposiderid bats. Further investigations on the innervation patterns of nycterids, rhinopomatids, and emballonurids that also have tracheal chambers (Denny [26]) are needed to test this hypothesis.

Prenatal development of the hyolaryngeal complex in horseshoe bats and in mice

We found that the hyolaryngeal complex reached adult morphology in bats and mice at the early fetal stage (Figs. 3A, 4A). The bilaterally extended lesser and greater horns of the hyoid in horseshoe bats became evident at an earlier stage than those in CS17. In humans, the second pharyngeal cartilage forms the elongated lesser horn of the hyoid at Carnegie Stage 18, followed by the development of the greater horn of the hyoid [61]. These cases suggest that the elongation of each horn of the hyoid is due to chondrocyte proliferation during the early fetal stage. We also confirmed that the thyrohyoid muscle increasingly develops toward the rostral side and merges at the median line in mice but not in horseshoe bats

(Fig. 4E, F). Around Carnegie Stage 20 in humans, the thyrohyoid muscle connects the greater horn of the hyoid and the thyroid cartilage [62], similar to rhinolophids. Together, the loosened hyoid–larynx connection of rhinolophids may result from differences in the initial construction of the thyrohyoid muscle, at least until CS17.

Our observations confirmed that each intrinsic laryngeal muscle became distinguishable at CS17 in bats and E14.5, in mice (Figs. 3 and 4). The time at which patterning of the intrinsic laryngeal muscles occurs in mice is consistent with the observations in the mouse embryo [63]. We also found that the left and right components of the dorsal cricoarytenoid muscle were present at the boundary of the sagittal crest, similar to CS17 (Fig. 4A). In mice, the dorsal cricoarytenoid muscle develops as a single muscle and is not divided by the sagittal crest throughout ontogeny (Fig. 4E–L). Because this pattern has also been described in rat embryos [64], a single dorsal cricoarytenoid muscle is likely to be conserved in rodents. In humans, the posterior cricoarytenoid muscle develops from two independent muscles and maintains a separate morphology until adulthood [65]. These facts suggest that the dorsal cricoarytenoid muscle of the horseshoe bat is not secondarily separated by the projection of the sagittal crest, but originally has two developmental centers. Despite less-documented myogenesis in non-model organisms, separated dorsal cricoarytenoid muscles in adults have been reported in elk, red deer [5], minipig [66], and horses [67]. Therefore, it is possible that a single dorsal cricoarytenoid muscle in mice is the derived phenotype in mammals, and the separated muscle in horseshoe bats is a synapomorphic trait in laurasiatherians.

We observed that the rostral tip of the cranial arch of the cricoid cartilage projected to split the cricothyroid muscle in horseshoe bats (Fig. 5D, G). The ventral component of the cricothyroid muscle was attached to the ventral side of the cranial arch, and the muscular wings of the cricoid cartilage were formed at CS20.5. Contrary to its development in mice, the ventral part of the cricothyroid muscle appeared to be newly formed and merged with the dorsal part (Fig. 5D). Therefore, the hypertrophied cricothyroid muscle in horseshoe bats may not be established by the expansion of a single component, but by the fusion of the original cricothyroid muscle and novel muscle components. Considering that this muscle is also attached to the lateral tracheal chamber, this pattern may be unique to rhinolophid and hipposiderid bats. The cricothyroid muscle of laryngeally echolocating bats has been reported to be hypertrophied [26] and capable of high-speed contraction in a few species (*Myotis daubentonii* [19] and *Myotis lucifugus* [68]). Although the early development of the cricothyroid muscle has not

yet been documented in other laryngeally echolocating lineages, the present study implies that the hypertrophied cricothyroid muscle is established through different developmental pathways among lineages with different biosonar pulse generation capabilities. Moreover, combined with observations in postnatal individuals (Fig. 1), the development of the cricothyroid muscle may proceed until birth. A similar pattern has been reported in horseshoe petrosal, in which the size growth is unusually prolonged until sexual maturation, leading to a remarkably enlarged cochlea in horseshoe bats [37]. The present study implies that the development of multiple organs related to both the reception and emission of biosonar sounds is prolonged concomitantly with the sophistication of laryngeal echolocation in horseshoe bats.

On the embryonic origins of the tracheal chambers in horseshoe bats

We have described the early development of the lateral and dorsal tracheal chambers in horseshoe bats (Fig. 6). Immunohistochemistry for the Sox9 protein identified that the lateral and dorsal tracheal chambers developed by chondrocyte proliferation, such as the laryngeal cartilage (Fig. 6A-2). It has been hypothesized that tracheal chambers are formed by the modification of the tracheal ring (Denny et al. [26]). Histological observations indicated that the condensed chondrocyte mass comprising the lateral tracheal chamber originated from the ventral portion of the cricoid cartilage, whereas the tracheal rings had not yet chondrified (Fig. 6A). Thus, we suggest that the lateral and dorsal tracheal chambers are cricoid-derived laryngeal cartilages acquired in rhinolophids and hipposiderids due to the expansion of the caudal tip of the cricoid cartilage. It has been widely accepted that the rhinolophids and hipposiderids significantly radiate their bioacoustics strategy, as represented by the emission of HDC pulses [22] and DSC, allowing them to improve the accuracy of target localization [31]. Tracheal chambers are known to function as pulse amplifiers for the reinforcement of sound intensity because of their susceptibility to attenuation during emission through the nostrils [26, 29]. The concept of "key innovations" has been defined in evolutionary developmental biology as a substantial change of the characters that have triggered lineage diversification [69, 70]. In accordance with this definition, tracheal chambers found explicitly in laryngeally echolocating bats emitting pulses with their nostrils (rhinolophids, hipposiderids, nycterids, rhinopomatids, and emballonurids) should be regarded as key innovations in the larynx. In light of this, key innovations in the cricoid cartilage might have led to the sophistication of laryngeal echolocation in tandem with the acquisition of HDC and DSC capabilities.

Genetic studies have reported that the development of respiratory organs such as the larynx, trachea, and lungs is regulated by the expression of *Fgf10* [71], *chordin* [72], *Fuz, Gli3* [73], *β-catenin* [74], and *Tbx1* [75]. In particular, it has been reported that *Fgf10* knockout experiments induce the disorganization of mesenchymal cells at the distal end of the trachea and the absence of lung buds [71]. Given this, changes in the genetic factors represented by *Fgf10* might result in changes in the distribution of mesenchymal cells, thereby inducing the expansion of the cricoid cartilage in horseshoe bats. Further investigations using gene expression analysis are required to uncover the genetic basis underlying the evolution of tracheal chambers.

Pre- and postnatal ossification of the hyolaryngeal apparatus

This study described hyoid ossification (Figs. 7 and 9) and estimated the relative ossification timing of each element (Fig. 8). The timing of ossification of the hyoid components in horseshoe bats was accelerated relative to that of mice, except for the basihyal component (Fig. 8), although hyoid condensation was simultaneously observed at the early fetal stage in both species (Fig. 4). This indicates that the ossification sequence was not necessarily consistent with the chondrification sequence. In mice, the basihyal was the only hyoid component to ossify at birth (Fig. 9G), whereas in horseshoe bats, all bony elements in the hyoid apparatus were already ossified (Fig. 9A). In laryngeally echolocating bats, the stylohyal bone is articulated with an ectotympanic [34], which possibly facilitates the transmission of the ongoing signal into the inner ear through bone conduction [42]. A recent biomechanical analysis revealed that the closer the bony element was to the basihyal bone, the higher the sound pressure is (Snipes and Carter [42]). The ongoing echolocation pulse, which is produced in the larynx, transfers to the thyrohyal and basihyal regions and subsequently propagates into the ceratohyal, epihyal, stylohyal, and ectotympanic regions. Our results suggest that construction of the stylohyal-ectotympanic unit is preceded relatively by the thyrohyal–basihyal unit.

Our analyses revealed that the thyroid, cricoid, and arytenoid cartilages began mineralization immediately before birth in horseshoe bats. The cricoid and arytenoid cartilages were entirely mineralized, whereas mineralization of the thyroid cartilage was limited to the lateral and rostral parts, even in the adult stage (Fig. 7). The pattern of laryngeal mineralization in horseshoe bats contrasts with that in phyllostomid bats, which possess non-mineralized thyroid and arytenoid cartilages [26, 40, 46]. It has been suggested that laryngeal cartilage, which requires dynamic motion, tends to be more mineralized than

static cartilages such as the cricoid cartilage [46]. Horse-shoe bats produce high-intensity sounds in contrast to phyllostomids that emit low-intensity pulses [76]; thus, the highly mineralized cricoid and arytenoid cartilages in horseshoe bats would provide physical support for the superfast contraction of the hypertrophied cricothy-roid muscle. Considering that the mineralized lateral and rostral parts of the thyroid cartilage correspond to the attachment sites of the cricothyroid and thyroarytenoid muscles, respectively (Fig. 1A–D), limited mineraliza-tion may be due to the high functional requirements of these two muscles for laryngeal echolocation. The lim-ited mineralization of the thyroid cartilage, on the other hand, may be due to the high functional requirements of the cricothyroid and thyroarytenoid muscles for pulse generation. Indeed, phyllostomid bats without mineral-ized thyroid and arytenoid cartilage possess a relatively smaller cricothyroid muscle than other echolocating bats [28, 45]. Taken together, the differences in the mineral-ized laryngeal cartilage between the rhinolophids and hipposiderids groups and phyllostomids may imply that these two nasally echolocating lineages employ different morphologies and kinetics of the laryngeal muscle during laryngeal echolocation.

Mineralization of the lateral and dorsal tracheal cham-bers began at P14 and P21, respectively (Figs. 6E, F, 7 B, C). Although the tracheal chambers do not have attachment sites for the other muscles, except for the cricothyroid muscle, almost all the tracheal chambers were mineralized, such as the cricoid and arytenoid car-tilages. Chondrification was already evident at CS17 (Fig. 6A), and connections between the lateral tracheal chamber and cricoid cartilage and between the dorsal tracheal chamber and third tracheal ring were estab-lished until CS22 (Fig. 6B). The air sac in the tracheal chambers prevents the echolocation pulse from being reflected from the lungs toward the auditory organs [77]. The tracheal chambers would vibrate during the emis-sion of the biosonar pulse and are exposed to mechanical stress, thereby leading to mineralization of the entire car-tilage. Following the mineralization of the other laryngeal cartilages, the structurally strengthened cartilages would increasingly reinforce the capability of biosonar pulse emission.

Relationship between development and pulse ontogeny
We confirmed that no echolocation pulses were observed at the newborn (P0) stage (Fig. 12), as reported in a previ-ous study [78]. In the P0 specimen, the basihyal bone was not fused with the thyrohyal bone, and each component of the lesser horn (ceratohyal, epihyal, and stylohyal) of the hyoid was not in contact, indicating that the capabil-ity of bone conduction was still immature at this stage (Figs. 6D, 7A). Furthermore, mineralization of the rostral part of the thyroid cartilage, cranial arch of the cricoid cartilage, and lateral tracheal chamber was not observed
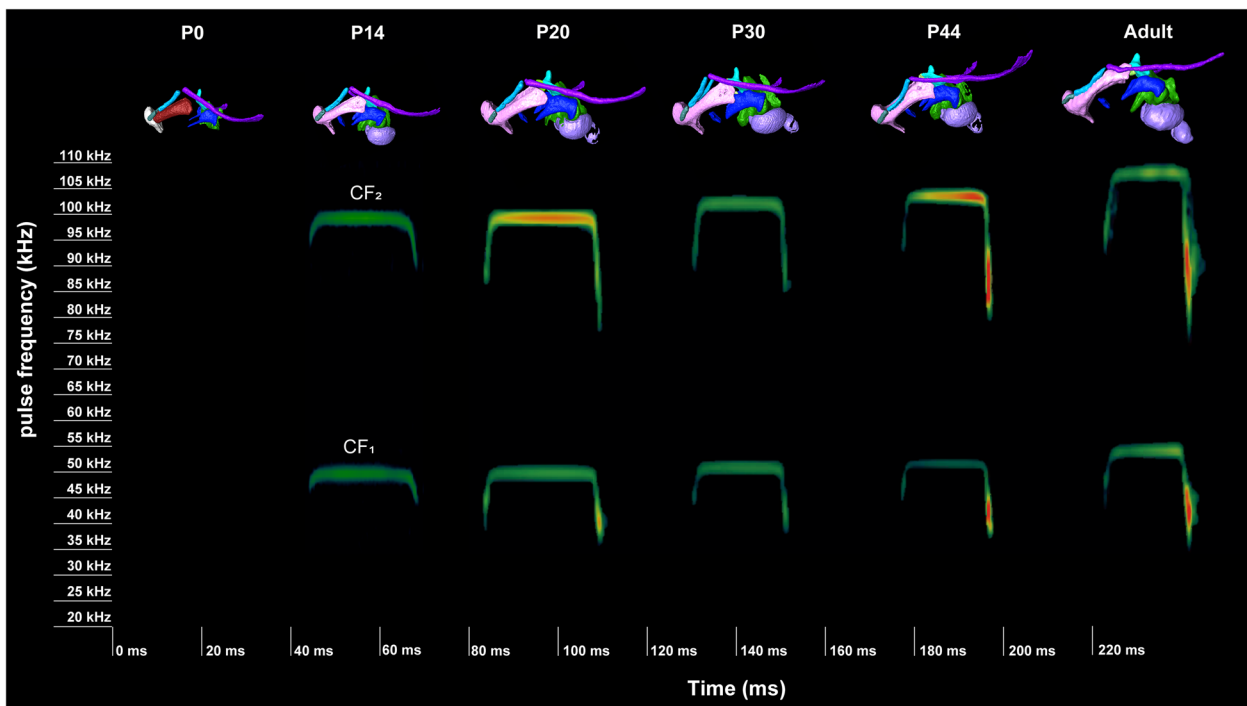

Fig. 12 Ontogeny of the hyolaryngeal apparatus morphology and the echolocation pulse in *Rhinolophus pusillus*

at this stage. Because the basihyal–thyrohyal unit is most susceptible to sound pressure during laryngeal echolocation [42], the establishment of a strongly supported hyoid apparatus may be essential for the acquisition of biosonar pulse emission. The echolocation pulse is known to gradually develop from spontaneous calls used for mother–infant communication when juvenile individuals start powered flights [79]. Our findings suggest that the progression of laryngeal mineralization reinforces the rapid contraction of the intrinsic laryngeal muscles and consequently allows bat pups to distinguish the echolocation pulse from precursor calls. As tracheal chambers improve the sound intensity for laryngeal echolocation [26, 29, 77], well-mineralized tracheal chambers are required for the maturation of high-intensity pulses in horseshoe bats [1]. Therefore, in contrast to phyllostomids with low-intensity calls, the structural demand for the endurance of high-intensity signals is likely reflected in the progressive mineralization of the laryngeal cartilages of horseshoe bats.

We detected positive allometric patterns in all laryngeal cartilages compared to the cubed geometric mean (Fig. 10A–D). Regarding the cricoid cartilage, mineralization occurred within a short period immediately before birth (Fig. 10A). The cricoid cartilage is surrounded by the dorsal cricoarytenoid and cricothyroid muscles (Fig. 1B–D). We suggest that the precedence of the mineralization of the cricoid cartilage allows horseshoe bats to promptly reinforce the foundation of their superfast muscles. Moreover, the regression slope of the peak frequency of the echolocation pulse against the cubed geometric mean showed a negative allometric pattern (Fig. 10E, F). The correlation between body mass and sound frequency in mammals has been widely recognized as size–frequency allometry [80]. A previous study reported a significant positive relationship between forearm length and the frequency of the second harmonic pulse in the juvenile stage of *R. cornutus* [79] and *R. ferrumequinum* [81], but the negative allometric pattern from juvenile to adult stages found in the present study (Fig. 10) indicates that the pulse peak frequency does not necessarily increase at a rate similar to that of body size.

Our GLM analyses identified significant correlations between the cricoid thyroid, arytenoid cartilage, and tracheal chambers and the peak frequencies of the CF_1 and CF_2 components (Fig. 11). Since the mineralized parts of the laryngeal cartilage correspond to the attachment sites of the cricothyroid, thyroarytenoid, and cricoarytenoid muscles (Fig. 1A–D), these four laryngeal cartilages are likely to be highly susceptible to mechanical stress during muscle contraction. The generation of high-frequency sounds requires superfast muscle (i.e., the cricothyroid muscle) control of the vocal cords [19]. Abduction of the glottis to vibrate the vocal fold involves contraction of the dorsal cricoarytenoid muscle. It has been suggested that tracheal chambers contribute to sound intensity [26, 29, 52, 77]. Given that the ventral part of the cricothyroid muscle is attached to the lateral tracheal chambers, mineralization of the tracheal chambers can be promoted by superfast contraction of this muscle. Thus, the ontogeny of the pulse peak frequency was also reflected in the mineralization of the tracheal chambers. Hence, we suggest that the ontogeny of the peak frequency of the echolocation pulse is underpinned by the mineralization of these four laryngeal cartilages in horseshoe bats.

Implications for the evolution of the laryngeal echolocation in bats

We found that horseshoe bats possess a unique morphology, such as hypertrophied intrinsic laryngeal muscles (Fig. 1B) and a sagittal crest (Fig. 1C), as reported in previous studies [26, 44]. Regarding hyoid morphology, we identified that horseshoe bats possess the following five hyoid elements: basihyal, thyrohyal, ceratohyal, epihyal, and stylohyal (Figs. 1A–D, 3A–C, 6, 7). A novel pattern of innervation of the cranial laryngeal nerve was also identified using immunohistochemical staining (Fig. 3). Considering that the novel branch of the cranial laryngeal nerve runs into the ventrally expanded portion of the cricothyroid muscle, the hypertrophied cricothyroid muscle comprises two components: (1) homologous cricothyroid muscle in general mammals and (2) novel muscle acquired along with the acquisition of the tracheal chambers in horseshoe bats (Fig. 3). Our findings corroborate that the evolution of sophisticated biosonars, such as DSC, in horseshoe bats might be underpinned by morphological changes in the hyolaryngeal complex.

Hyoid morphology has been recognized as a key component of laryngeal echolocation [33, 34, 39, 42, 43, 47, 52, 58, 82–85]. Regarding the entire morphology of the hyoid apparatus in bats, it has been suggested that the number of hyoid components varies among lineages [45]. In contrast to the hyoid apparatus with the segmented lesser cornua in horseshoe bats (Figs. 1A–D, 6, 7A–C), for example, vespertilionid bats do not have the epihyal and ceratohyal, forming the lesser cornua only with the stylohyal bone [86]. The genus *Myotis*, on the other hand, is known to have a lesser cornua formed by the two bony elements [86], although the homology of each component in horseshoe bats is still unclear. Because morphological differences in the hyoid apparatus are related to variations in the efficiency of sound propagation [42], morphological changes in the hyoid apparatus may contribute to the diversification of acoustic properties, such as sound frequency, duration, and intensity, in laryngeally echolocating bats.

The present study identified unique characteristics such as a possibly novel branch of the cranial laryngeal nerve in rhinolophids. This lineage may have achieved pulse generation with different laryngeal kinetics of the superfast muscle compared to that of yangochiropterans [19]. Regarding pteropodids, the sister clade of the rhinolophoids within the yinpterochiropterans, the morphology of their laryngeal muscles has been reported to be similar to that of the vespertilionid bats in the yangochiropterans, rather than that of the rhinolophoids [52, 59]. Given this, laryngeal development may also be divergent within lineages with different echolocation capabilities, as well as the petrosal and stylohyal (Nojiri et al. [39]). The molecular study detected positive selection of the hearing genes of the ancestral branches of bats, suggesting that the common ancestor of bats employed primitive sonar, such as the lingual echolocation of the genus *Rousettus*, and then rhinolophoids and yangochiropterans acquired sophisticated laryngeal echolocation [87]. To date, there have been few studies on laryngeal development in bats, especially in pteropodids and yangochiropterans, making this hypothesis difficult to validate. This study reveals several key characteristics involved in the generation of echolocation pulses. We identified significant differences in the morphology of the mineralized laryngeal cartilage and the presence of the echolocation pulse between P0 and P14 specimens. For example, the emission of the echolocation pulse was confirmed after P14, at which the lateral tracheal chambers started mineralization (Fig. 9C, D), possibly contributing to the acquisition of the echolocation pulse production capability. Given this, the macroevolutionary changes in the cricoid cartilage and acquisition of tracheal chambers might have co-evolved to some extent with the acquisition of sophisticated biosonar in horseshoe bats. In subsequent studies, investigations of the commonality and disparity of hyolaryngotracheal morphology in extinct and extant bats would provide key insights into the evolutionary origins of laryngeal echolocation and diversification of biosonar in bats.

Conclusions

Three-dimensional reconstruction of the hyolaryngeal apparatus revealed the unique morphology of the cricoid cartilage, intrinsic laryngeal muscle, and cranial laryngeal nerve in horseshoe bats. The present study suggests that the sagittal crest of the cricoid cartilage and the separated dorsal cricoarytenoid muscles may be key features involved in echolocation pulse generation. Laryngeally echolocating bats are characterized by hypertrophied intrinsic laryngeal muscles, including the cricothyroid muscles, with superfast contractions. We provide a new perspective that the hypertrophied cricothyroid muscle

of horseshoe bats comprises homologous muscles in mammals and possibly novel components acquired in rhinolophids and hipposiderids, which may have served as key innovations in the adaptive radiation of these HDC bats. This drastic morphological innovation is possibly in concert with the acquisition of tracheal chambers, allowing them to conduct sophisticated biosonar with high accuracy for target localization. In addition, we found that the maximum frequency of the echolocation pulse was significantly correlated with mineralization of the cricoid and arytenoid cartilages. Given the acoustic diversity in laryngeally echolocating bats, it is possible that the postnatal mineralization of each laryngeal cartilage may independently regulate each acoustic property. Future studies integrating the hyolaryngeal development of pteropodids, yangochiropterans, and other rhinolophoids will offer insights into the relationship between variations in sound properties and hyolaryngeal morphology and improve our understanding of how morphological changes in the hyolaryngeal apparatus shape acoustic diversity in bats.

Methods

Data acquisition

A total of 32 specimens of the genus *Rhinolophus* species (*R. pusillus*, $n=28$; *R. malayanus*, $n=4$) and ten specimens of C57/BL6 mice (*Mus musculus*) were studied. The fetal and postnatal specimens of *R. pusillus* were collected by the authors in Japan and Vietnam. *Rhinolophus pusillus* from Japan was collected under the permission granted by the Gosen Local Government in Japan (No. 1–4-2021) and is stored at the University of Tsukuba (UT). The fetal specimens of *R. malayanus* were collected by the authors during field sampling in Vietnam under permission granted by the An Giang Province People's Committee in Vietnam (No. 497/VPUBND-NC and No. 5893/VPUBND-KTN) and the Vietnam Administration of Forest, belonging to the Ministry of Agriculture and Rural Development (No. 1072/TCLN-BTTN and No.326/TCLN-BTTN). *Rhinolophus pusillus* from Japan and Vietnam are considered to compose a single species, and geographic variation of the hyolaryngeal morphology was not detected between individuals from Japan and those from Vietnam. Our postnatal samples of *R. pusillus* comprehensively covered the overall ontogeny of the echolocation pulse, but some stages of prenatal specimens were lacking to describe the ossification sequence of the hyolaryngeal bony components. Therefore, fetal specimens of *R. malayanus*, both of which are members of the same genus *Rhinolophus* [88], were additionally included. The examined specimens of *R. pusillus* and *R. malayanus* were first confirmed to show no significant difference in qualitative hyolaryngeal morphology.

Animal ethics for mice sampling and experiments were approved at Tokyo Medical and Dental University, Japan (A2019-060C3 and A2021-198A). All experiments were conducted following the ARRIVE guidelines following the Japanese law on animal welfare. All pregnant individuals captured in this study were euthanized by isoflurane inhalation. Fetal bat specimens were staged following Cretekos Stage (CS) [89]. The postnatal stage of bats was estimated by the time when the first birth was observed in the reproductive colony. The details of all specimens are summarized in Table 3. Fetal specimens examined in this study include stages from CS16 to CS24 (*R. pusillus*: CS16, 17, 18, 19, 20, 21, 22, 23, 24; *R. malayanus*: CS18, 20.5, 22). Postnatal specimens, all of which were *R. pusillus*, covered postnatal day 0, 14, 21, 30, 45, and adult. One adult individual of *R. pusillus* was loaned from the curatorial collection held in Kanagawa Prefectural Museum of Natural History (KPMNH), and all samples of *R. malayanus* from the curatorial collection held in the Institute of Ecology and Biological Resources, Vietnamese Academy of Science and Technology (IEBR). All mouse fetuses from E14.5 to E18.5 and postnatal specimens from P0 to adult (*n*=10) were collected at Tokyo Medical and Dental University (TMDU). Pregnant mice were killed by cervical dislocation. The collected specimens were fixed using a mixture of ethyl alcohol:acetic acid:formalin (6:3:1) and stored in 70% ethyl alcohol. Specimens used in this study are summarized in Table 3.

Three-dimensional reconstruction of hyolaryngeal morphology

To investigate the development of the hyolaryngeal apparatus in the fetal and postnatal stages, we used microcomputed tomography (micro-CT) at University of Tsukuba (inspeXio SMX-90CT Plus, Shimadzu Corporation, Tokyo) and University Museum of University of Tokyo (TXS225-ACTIS, Tesco, Tokyo) with a 70 kV source voltage and 100 mA source current. To visualize the cartilage and muscle for postnatal individuals (P0, 14, 21, 30, 45, and adult), the diffusible iodine-based contrast-enhanced CT technique [55] was conducted. This method has been shown to effectively allow us to non-destructively investigate the morphology of bat soft tissues in detail [38, 39, 90–93]. Specimens were stained with 1% iodine in ethanol for at least 48 h and up to 14 days. The morphology of each hyolaryngeal component was manually segmented from the aligned serial tissue sections (Fig. 13) and micro-CT images (Fig. 14) in Amira 5.3 Table 4.

Histology

Serial tissue sections were prepared to reconstruct the detailed morphology that is still difficult to visualize by the diffusible iodine-based contrast-enhanced CT. Three stages of bats (CS17, CS20.5, CS22) and mice (E14.5, E16.5, E18.5) were dehydrated in ethanol series and embedded in paraffin wax. Sections were cut at 6 µm for the CS17 bat and E14.5 mouse, and 7 µm for the other stages. For immunohistochemistry (IHC) staining of CS22 of *R. malayanus* and E18.5 of mice, mouse anti-acetylated tubulin (mouse monoclonal anti-acetylated tubulin, no. T7451; Sigma-Aldrich Japan, Tokyo) was used to visualize the innervations. For CS17 of *R. pusillus*, anti-Sox9 (rabbit polyclonal antibody, no. AB5535; Sigma-Aldrich Japan, Tokyo) was used to visualize the chondrifications. The immunoreaction was visualized by the secondary antibody conjugated with the anti-mouse IgG-Biotin antibody. The sections were then stained with Alcian blue and hematoxylin to identify the cartilages and muscles following the standard staining protocols. The obtained serial sections were aligned and then each targeted organ was manually segmented using Amira 5.3 (Visage Imaging GmbH).

Measurements

To examine the allometric growth of the mineralized components against overall skull size in horseshoe bats, the skull size and volume of the mineralized laryngeal cartilages (cricoid, arytenoid, thyroid cartilages, lateral, and dorsal tracheal chambers) were measured using the Surface Area Tool and 3D Length Tool in Amira 5.3. As the index of overall skull size [94], the geometric mean (GM) was calculated from the skull length (SL), skull height (SH), and skull width (SW) as

$$GM^3 = SL * SH * SW.$$

The cubed GM (GM^3) was used as the index of the skull size in our allometric analyses. Skull length (SL) was measured as the distance from the rostral tip of the premaxilla to the ventral end of the interparietal in the sagittal plane. Skull height (SH) was measured as the distance from the midpoint of the cranial tip of the left and right parietals to the rostral tip of the basioccipital. Skull width (SW) was taken as the distance of the bilateral tip of the squamosal.

Bioacoustics

Echolocation pulses of P0 (*n*=3), P14 (*n*=3), P21 (*n*=1), P30 (*n*=2), P45 (*n*=1), and adult (*n*=1) individuals were recorded, and sonograms were obtained during the field sampling using Echo Meter Touch 2 Pro (Wildlife Acoustics Inc., Concord, MA). The mean of the sound frequency of the first harmonic (CF_1) and second harmonic (CF_2) pulse of the constant frequency (CF) was taken as the index for the capability of the biosonar pulse emission using Kaleidoscope Pro Analysis Software (Wildlife Acoustics Inc., Concord, MA).

Table 3 All specimens examined in this study

Species	ID	Storage	Stage	Bone micro-CT	diceCT	Tissue section
Mus musculus	NT22-002	TMDU	E14.5			x
Mus musculus	NT22-003	TMDU	E16.5			x
Mus musculus	JP19-001	TMDU	E17.5	x		
Mus musculus	NT22-004	TMDU	E18.0			x
Mus musculus	NT22-005	TMDU	Postnatal day 0	x		
Mus musculus	NT22-011	TMDU	Postnatal day 0		x	
Mus musculus	NT22-007	TMDU	Postnatal day 7	x		
Mus musculus	NT22-008	TMDU	Postnatal day 14	x		
Mus musculus	NT22-012	TMDU	Postnatal day 14		x	
Mus musculus	NT22-010	TMDU	Adult	x		
Rhinolophus pusillus	JP20-052	UT	CS16	x		
Rhinolophus pusillus	JP20-044	UT	CS17	x		
Rhinolophus pusillus	JP20-055	UT	CS17			x
Rhinolophus pusillus	JP20-039	UT	CS18	x		
Rhinolophus pusillus	QN043	IEBR	CS19	x		
Rhinolophus pusillus	QN041	IEBR	CS20	x		
Rhinolophus pusillus	B160413-4	IEBR	CS21	x		
Rhinolophus pusillus	JP21-032	UT	CS22	x	x	
Rhinolophus pusillus	XL2016-25	IEBR	CS22	x		
Rhinolophus pusillus	VN17-299	IEBR	CS23	x		
Rhinolophus pusillus	B200413-7	IEBR	CS24	x		
Rhinolophus pusillus	JP21-047	UT	Postnatal day 0	x		
Rhinolophus pusillus	JP21-073	UT	Postnatal day 14	x		
Rhinolophus pusillus	JP21-074	UT	Postnatal day 14	x		
Rhinolophus pusillus	JP21-075	UT	Postnatal day 14	x	x	
Rhinolophus pusillus	JP22-067	UT	Postnatal day 14	x		
Rhinolophus pusillus	JP22-068	UT	Postnatal day 14	x		
Rhinolophus pusillus	JP22-082	UT	Postnatal day 21	x		
Rhinolophus pusillus	JP21-083	UT	Postnatal day 21	x		
Rhinolophus pusillus	JP21-091	UT	Postnatal day 21		x	
Rhinolophus pusillus	JP21-100	UT	Postnatal day 30	x	x	
Rhinolophus pusillus	JP21-101	UT	Postnatal day 30	x		
Rhinolophus pusillus	JP21-104	UT	Postnatal day 45	x	x	
Rhinolophus pusillus	JP21-025	UT	Adult		x	
Rhinolophus pusillus	KPMNH2937	IEBR	adult	x		
Rhinolophus malayanus	VN20-032	IEBR	CS18	x		
Rhinolophus malayanus	VN20-054	IEBR	CS18	x		
Rhinolophus malayanus	VN19-057	IEBR	CS20.5			x
Rhinolophus malayanus	VN19-029	IEBR	CS22			x

Ossification heterochrony

To examine the temporal specificity of the hyolaryngeal ossification in horseshoe bats, the relative ossification timing of the hyolaryngeal components (arytenoid cartilage, basihyal, ceratohyal, corniculate cartilage, cricoid cartilage, epihyal, stylohyal, thyrohyal, thyroid cartilage, dorsal and lateral tracheal chambers) was estimated. The ossification sequence of 31 craniocervical elements (alisphenoid, arytenoid cartilage, basihyal, basioccipital, basisphenoid, ceratohyal, corniculate cartilage, cricoid cartilage, dentary, dorsal and lateral tracheal chambers, ectotympanic, epihyal, exoccipital, frontal, goniale, jugal, lacrimal, maxilla, nasal, orbitosphenoid, palatine, parietal, petrosal, premaxilla, presphenoid, pterygoid, squamosal, stylohyal, supraoccipital, thyroid cartilage, thyrohyal, and vomer) was documented
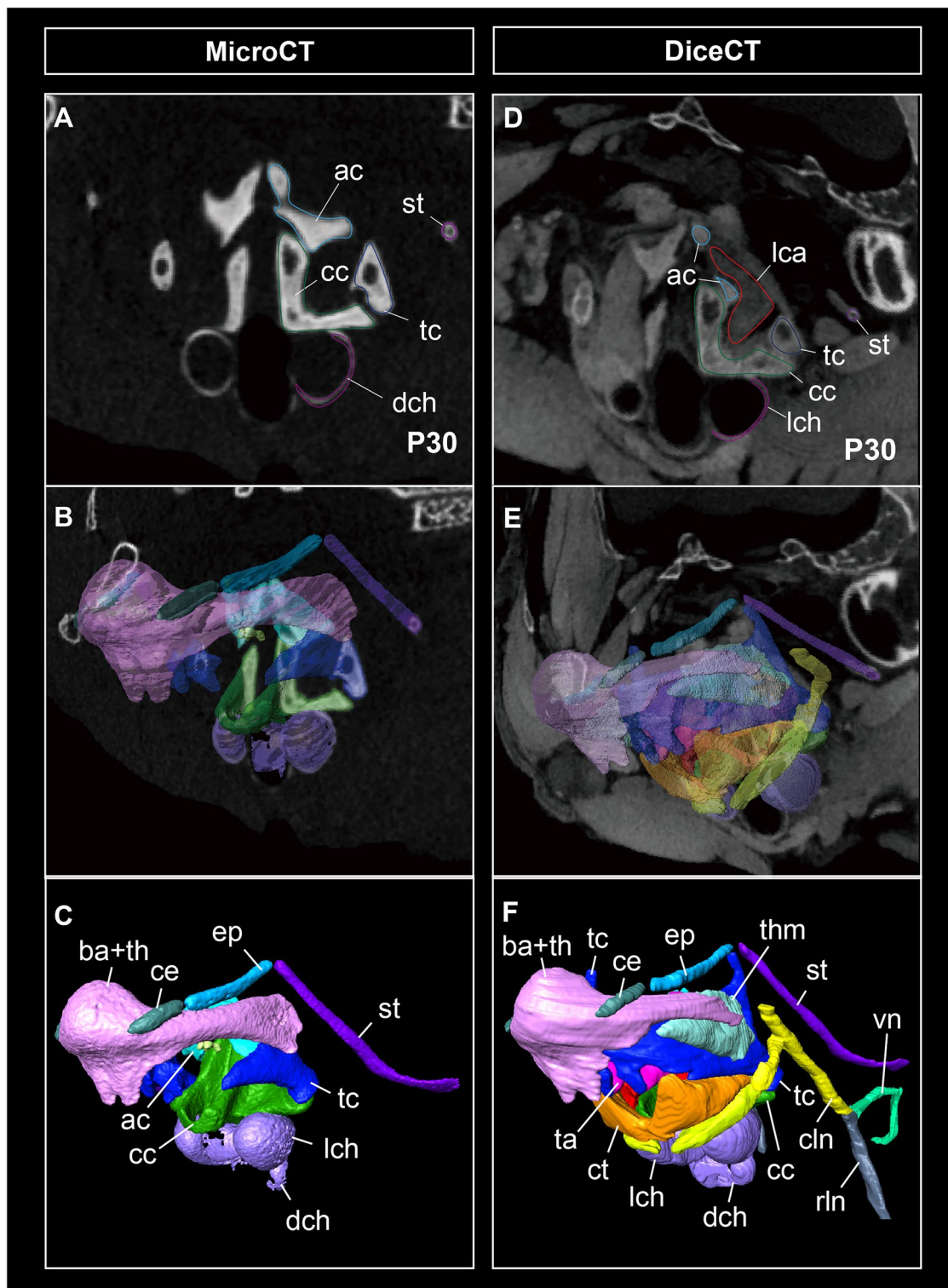
Fig. 13 The three-dimensional reconstruction procedure of the hard tissue and soft tissue of the hyolaryngeal apparatus in postnatal day 30 of *Rhinolophus pusillus*. **A** One example of the tomographic image obtained from micro-CT scanning without staining. **B** Three-dimensionally reconstruction process of the morphology of the hyolaryngeal cartilages with the tomographic images. **C** Three-dimensionally reconstructed morphology of the hyolaryngeal cartilages. **D** One example of the tomographic image obtained from diffusible iodine-based contrast-enhanced CT method. **E** Three-dimensionally reconstruction process of the morphology of the hyolaryngeal cartilages with the tomographic images. **F** Three-dimensionally reconstructed morphology of the hyolaryngeal cartilages, intrinsic laryngeal muscles, and vagus nerve (cranial nerve X). Left side of the hyolaryngeal morphology is shown
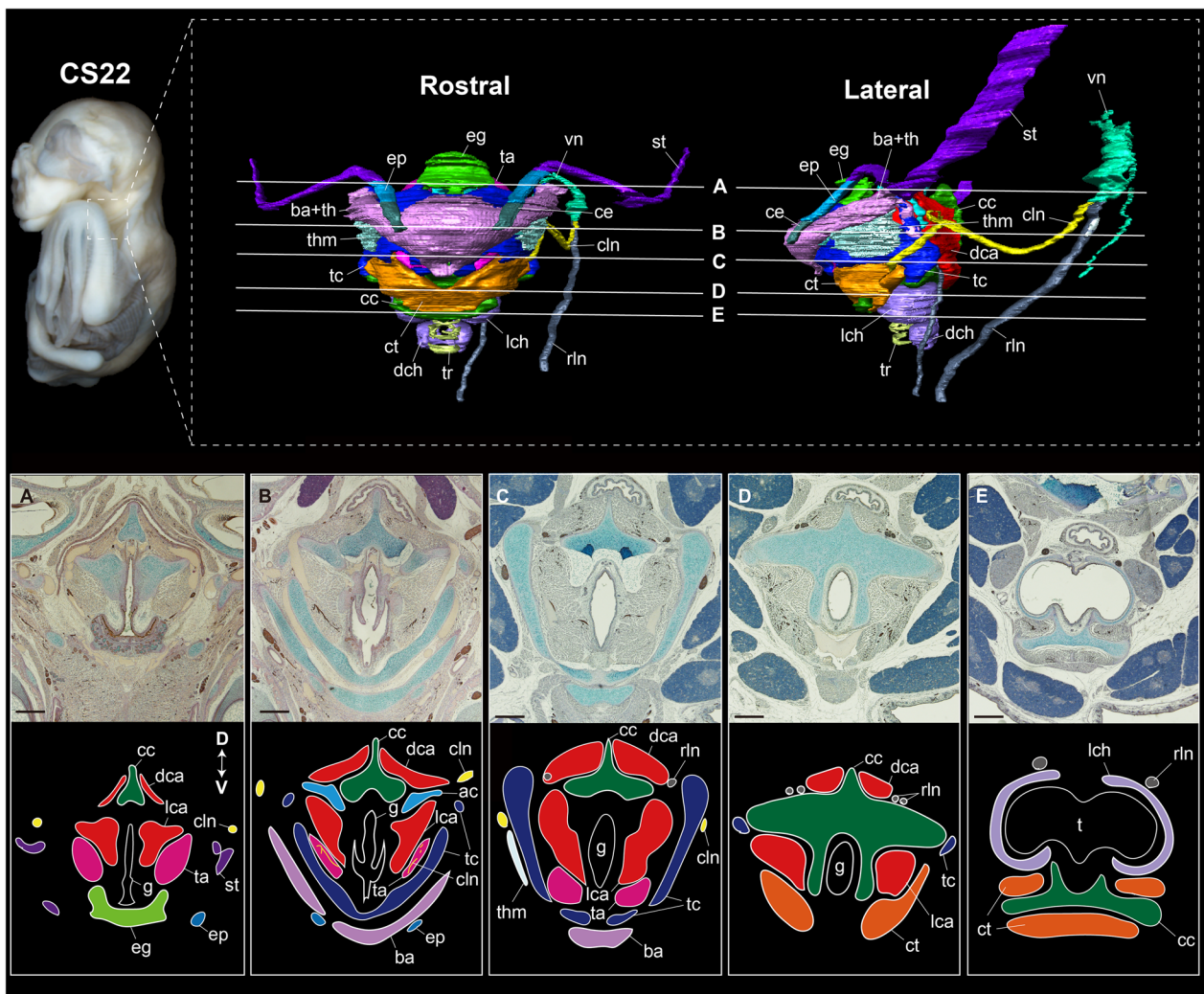
Fig. 14 The three-dimensional reconstruction procedure of the gross anatomy of the hyolarynx of the bat fetus (CS22; *Rhinolophus pusillus*) with serial tissue sections. All sections were immunostained with the acetylated tubulin antibody to visualize the nerves. Left side of the hyolarynx is shown in the lateral view. After immunostaining, all sections were additionally stained with alcian blue and hematoxylin. Scale bars = 500 µm. See text for abbreviations

for *Rhinolophus* species and *M. musculus*. To examine the relative ossification timing of each bony component and allow interspecific comparison, the rank of each ossification event was scaled as

$$\frac{(r-1)}{(r_{\max}-1)},$$

in which r is the absolute rank of each ossification event, and $r_{\max}$ is the total number of ranks for each species. The scaled relative values are distributed between 0 and 1. As the sequence resolution can affect the results in this approach, >3 ranks were documented for each species following [95].

Statistics

All statistical analyses were performed in PAST4. To examine the size allometry of the volume of the mineralized laryngeal cartilages, the reduced major axis (RMA) regression analysis was conducted. To rescale the data and handle them on a common scale, the volume of the cricoid (CV), thyroid (TV), arytenoid (AV), and lateral tracheal chamber (CH) were $\log_{10}$-transformed and regressed against $\log_{10}$-transformed GM^3. Furthermore, the regression line of the maximum frequency of the log10-transformed CF_1 and CF_2 components against log10-transformed GM^3 was also obtained. Given that the RMA

Table 4 Summary of measurements in each specimen in this study

Species	ID	Stage	GM³ (mm³)	First harmonic (kHz)	Second harmonic (kHz)	Cricoid cartilage volume (mm³)	Thyroid cartilage volume (mm³)	Arytenoid cartilage volume (mm³)	Lateral tracheal chamber volume (mm³)
Rhinolophus cornutus	JP21-045	Postnatal day 0	572.26			0.80	0.18	0.11	
Rhinolophus cornutus	JP21-046	Postnatal day 0	520.08			0.62	0.20	0.11	
Rhinolophus cornutus	JP21-047	Postnatal day 0	586.54			0.86	0.27	0.17	
Rhinolophus cornutus	JP21-073	Postnatal day 14	623.39	49.99	99.98	0.85	0.31	0.19	0.21
Rhinolophus cornutus	JP21-074	Postnatal day 14	645.35	49.58	99.20	0.93	0.37	0.22	0.27
Rhinolophus cornutus	JP21-075	Postnatal day 14	595.82	49.90	99.93	0.86	0.34	0.23	0.19
Rhinolophus cornutus	JP21-083	Postnatal day 21	644.23	50.67	101.23	0.87	0.35	0.23	0.32
Rhinolophus cornutus	JP21-097	Postnatal day 30	681.38	51.28	102.67	0.99	0.35	0.29	0.32
Rhinolophus cornutus	JP21-100	Postnatal day 30	681.38	50.89	101.83	1.01	0.41	0.27	0.31
Rhinolophus cornutus	JP21-101	Postnatal day 30	671.22	50.92	101.92	0.95	0.36	0.24	0.32
Rhinolophus cornutus	JP21-104	Postnatal day 45	701.12	51.69	103.37	1.06	0.38	0.31	0.36
Rhinolophus cornutus	JP21-103	Adult		54.14	108.25				
Rhinolophus cornutus	NHKM2937-	Adult	704.82			1.37	0.53	0.34	0.57
Mus musculus	JP19-001	E17.5	222.02						
Mus musculus	NT22-005	Postnatal day 0	288.58						
Mus musculus	NT22-007	Postnatal day 7	712.25						
Mus musculus	NT22-008	Postnatal day 14	1323.15				0.04		
Mus musculus	NT22-010	Adult	1748.84			0.38	0.73		

provides the best-estimated regression between every population from which the sample is selected when the error variance is unknown and is not affected by the correlation coefficient of samples, the RMA analysis is considered to be more appropriate than other regression models [96, 97].

To investigate the relationship between the pulse frequency and mineralization of the laryngeal cartilages, the generalized linear model (GLM) with identity link analyses was conducted. GLM analysis allows us to accommodate different types of response variables using the link function for various probability distributions and include the multiple independent variables in model, thus controlling for potential confounding factors that may influence the relationship between pulse peak frequency and mineralized volume of the laryngeal cartilages [98]. In the GLM analysis, the pulse frequency of CF_1 and CF_2 was set as the response variable, and the log-transformed volume of the mineralized cricoid cartilage, thyroid cartilage, arytenoid cartilage, lateral tracheal chamber, and dorsal tracheal chamber was as the explanatory variable. Since the pulse peak frequency is a continuous variable, it was assumed to follow a normal distribution. The volume of each mineralized laryngeal cartilage was divided by the estimated skull volume to remove the effect of the skull size growth (relative cricoid cartilage volume: RCV, relative thyroid cartilage volume: RTV, relative arytenoid cartilage volume: RAV, and relative lateral tracheal chamber volume: RCHV).

Abbreviations

ac	Arytenoid cartilage
ba	Basihyal
cc	Cricoid cartilage
ce	Ceratohyal
cln	Cranial laryngeal nerve
co	Corniculate cartilage
cp	Corniculate process of the arytenoid cartilage
ct	Cricothyroid muscle
dca	Dorsal cricoarytenoid muscle
dch	Dorsal tracheal chamber
eg	Epiglottis
ep	Epihyal
ft	Foramen thyrohyoideum
g	Glottis
hc	Hyoid complex
lca	Lateral cricoarytenoid muscle
lch	Lateral tracheal chamber
mw	Muscular wing of the cricoid cartilage
pt	Protuberance of the thyroid cartilage
rln	Recurrent laryngeal nerve
sc	Sagittal crest of the cricoid cartilage
st	Stylohyal
t	Trachea
ta	Thyroarytenoid muscle
tc	Thyroid cartilage
tcac	Thyroid caudal cornua
tcrc	Thyroid cranial cornua
th	Thyrohyal
thm	Thyrohyoid muscle
tr	Tracheal ring
vn	Vagus nerve
vp	Vocal process of the arytenoid cartilage

Supplementary Information

The online version contains supplementary material available at https://doi.org/10.1186/s13227-024-00221-7.

> **Additional file 1.** The coding of the craniocervical ossification or calcification in all specimens of *Rhinolophus* sp. and *Mus musculus,* examined this study.
>
> **Additional file 2.** The ossification or calcification sequence of the craniocervical elements in all specimens of *Rhinolophus* sp. and *Mus musculus,* examined this study.
>
> **Additional file 3.** The relative timing of the ossification or calcification of the craniocervical elements in all specimens of *Rhinolophus* sp. and *Mus musculus,* examined this study.

Author contributions

TN, MT, and DK conceived the study. TN, DF, VTT, TF, FM, and DK collected rhinolophid samples from the fields. TN and DK collected pulse data. MT and TF collected mouse embryos. TN, MT, TF, and DK scanned the specimens using micro-CT and stained the serial tissue sections. TN and DK drafted the manuscript. TN conducted all the analyses. All authors provided insights and critically revised the manuscript.

Availability of data and materials

All data supporting the findings of this study are available from the corresponding authors.

Declarations

Ethics approval and consent to participate

Animal ethics for the experiments were approved by the Tokyo Medical and Dental University, Japan (A2019-060C3 and A2021-198A).

Consent for publication

Not applicable.

Competing interests

The authors declare no conflicts of interest.

Author details

[1]Graduate School of Medicine, Juntendo University, 2-2-1 Hongo, Bunkyo-Ku, Tokyo 113-8421, Japan. [2]Department of Molecular Craniofacial Embryology, Tokyo Medical and Dental University, 1-5-45 Yushima, Bunkyo-Ku, Tokyo 113-8549, Japan. [3]Department of Infectious Diseases and Public Health, Jockey Club College of Veterinary Medicine and Life Sciences, City University of Hong Kong, Hong Kong SAR, China. [4]The University of Tokyo Fuji Iyashinomori Woodland Study Center, Graduate School of Agricultural and Life Sciences, The University of Tokyo, 341-2 Yamanaka, Yamanakako, Yamanashi 401-05013, Japan. [5]Institute of Ecology and Biological Resources, Vietnam Academy of Science and Technology, No. 18, Hoang Quoc Viet Road, Cau Giay District, Hanoi, Vietnam. [6]Graduate University of Science and Technology, Vietnam Academy of Science and Technology, No. 18, Hoang Quoc Viet Road, Cau Giay District, Hanoi, Vietnam. [7]Research and Development Center for Precision Medicine, University of Tsukuba, 1-2 Kasuga, Tsukuba-Shi, Ibaraki 305-8550, Japan.

References

1. Fenton MB. Evolution of Echolocation. In: Adams RA, Pedersen SC, editors. Bat Evolution, Ecology, and Conservation. New York: Springer, New York; 2013. p. 47–70.
2. Ketten DR. The Marine Mammal Ear: Specializations for Aquatic Audition and Echolocation. In: Webster DB, Popper AN, Fay RR, editors. The Evolutionary Biology of Hearing. New York: Springer, New York; 1992. p. 717–50.
3. O'Connell-Rodwell CE, Arnason BT, Hart LA. Seismic properties of Asian elephant (Elephas maximus) vocalizations and locomotion. J Acoust Soc Am. 2000;108:3066–72.
4. Charlton BD, Frey R, McKinnon AJ, Fritsch G, Fitch WT, Reby D. Koalas use a novel vocal organ to produce unusually low-pitched mating calls. Curr Biol. 2013;23:R1035–6.
5. Frey R, Riede T. The anatomy of vocal divergence in North American Elk and European red deer. J Morphol. 2013;274:307–19.
6. Fitch WT. Vocal tract length and formant frequency dispersion correlate with body size in rhesus macaques. J Acoust Soc Am. 1997;102:1213–22.
7. Nishimura T. Comparative morphology of the hyo-laryngeal complex in anthropoids: two steps in the evolution of the descent of the larynx. Primates. 2003;44:41–9.
8. Nishimura T, Oishi T, Suzuki J, Matsuda K, Takahashi T. Development of the supralaryngeal vocal tract in Japanese macaques: implications for the evolution of the descent of the larynx. Am J Phys Anthropol. 2008;135:182–94.

9.   Zhang YS, Takahashi DY, Liao DA, Ghazanfar AA, Elemans CPH. Vocal state change through laryngeal development. Nat Commun. 2019;10:4592.

10. Bowling DL, Dunn JC, Smaers JB, Garcia M, Sato A, Hantke G, et al. Rapid evolution of the primate larynx? PLoS Biol. 2020;18: e3000764.

11. Fitch WT, de Boer B, Mathur N, Ghazanfar AA. Monkey vocal tracts are speech-ready. Sci Adv. 2016;2: e1600723.

12. Nishimura T, Tokuda IT, Miyachi S, Dunn JC, Herbst CT, Ishimura K, et al. Evolutionary loss of complexity in human vocal anatomy as an adaptation for speech. Science. 2022;377:760–3.

13. Landrau-Giovannetti N, Mignucci-Giannoni AA, Reidenberg JS. Acoustical and anatomical determination of sound production and transmission in West Indian (*Trichechus manatus*) and Amazonian (*T. inunguis*) manatees. Anat Rec. 2014;297:1896–907.

14. Borgard HL, Baab K, Pasch B, Riede T. The shape of sound: a geometric morphometrics approach to laryngeal functional morphology. J Mamm Evol. 2020;27:577–90.

15. Riede T, Coyne M, Tafoya B, Baab KL. Postnatal development of the mouse larynx. J Speech Lang Hear Res. 2020;63:2680–94.

16. He K, Liu Q, Xu D-M, Qi F-Y, Bai J, He S-W, et al. Echolocation in soft-furred tree mice. Science. 2021;372:eaay1513.

17. Lesch R, Schwaha T, Orozco A, Shilling M, Brunelli S, Hofer M, et al. Selection on vocal output affects laryngeal morphology in rats. J Anat. 2021;238:1179–90.

18. Smith SK, Burkhard TT, Phelps SM. A comparative characterization of laryngeal anatomy in the singing mouse. J Anat. 2021;238:308–20.

19. Elemans CPH, Mead AF, Jakobsen L, Ratcliffe JM. Superfast muscles set maximum call rate in echolocating bats. Science. 2011;333:1885–8.

20. Håkansson J, Mikkelsen C, Jakobsen L, Elemans CPH. Bats expand their vocal range by recruiting different laryngeal structures for echolocation and social communication. PLoS Biol. 2022;20: e3001881.

21. Teeling EC, Springer MS, Madsen O, Bates P, O'brien SJ, Murphy WJ. A molecular phylogeny for bats illuminates biogeography and the fossil record. Science. 2005;307:580–4.

22. Jones G, Teeling EC. The evolution of echolocation in bats. Trends Ecol Evol. 2006;21:149–56.

23. Yovel Y, Geva-Sagiv M, Ulanovsky N. Click-based echolocation in bats: not so primitive after all. J Comp Physiol A Neuroethol Sens Neural Behav Physiol. 2011;197:515–30.

24. Boonman A, Bumrungsri S, Yovel Y. Nonecholocating fruit bats produce biosonar clicks with their wings. Curr Biol. 2014;24:2962–7.

25. Pedersen SC. Morphometric analysis of the Chiropteran skull with regard to mode of echolocation. J Mammal. 1998;79:91–103.

26. Denny SP. The bat larynx. Scientific foundations of otolaryngology. 1976.

27. Griffiths TA, Smith AL. Systematics of emballonuroid bats (Chiroptera, Emballonuridae and Rhinopomatidae), based on hyoid morphology. Bull Am Soc Inf Sci. 1991;18:e0285271.

28. Griffiths TA, Koopman IKF, Starrett A. The Systematic Relationship of *Emballonura nigrescens* to other Species of Emballonura and to Coleura (Chiroptera: Emballonuridae). Am Mus Novit. 1991;2996:1–16.

29. Roberts LH. Variable resonance in constant frequency bats. J Zool. 1972;166:337–48.

30. Griffiths TA. Modification of m. cricothyroideus and the larynx in the Mormoopidae, with reference to amplification of high-frequency pulses. J Mammal. 1978;59:724–30.

31. Hiryu S, Katsura K, Lin L-K, Riquimaroux H, Watanabe Y. Doppler-shift compensation in the Taiwanese leaf-nosed bat (*Hipposideros terasensis*) recorded with a telemetry microphone system during flight. J Acoust Soc Am. 2005;118:3927–33.

32. Habersetzer J, Storch G. Cochlea size in extant chiroptera and middle eocene microchiropterans from messel. Naturwissenschaften. 1992;79:462–6.

33. Simmons NB, Seymour KL, Habersetzer J, Gunnell GF. Primitive early eocene bat from Wyoming and the evolution of flight and echolocation. Nature. 2008;451:818–21.

34. Veselka N, McErlain DD, Holdsworth DW, Eger JL, Chhem RK, Mason MJ, et al. A bony connection signals laryngeal echolocation in bats. Nature. 2010;463:939–42.

35. Davies KT, Maryanto I, Rossiter SJ. Evolutionary origins of ultrasonic hearing and laryngeal echolocation in bats inferred from morphological analyses of the inner ear. Front Zool. 2013;10:2.

36. Carter RT, Adams RA. Postnatal ontogeny of the cochlea and flight ability in Jamaican fruit bats (Phyllostomidae) with implications for the evolution of echolocation. J Anat. 2015;226:301–8.

37. Nojiri T, Werneburg I, Son NT, Tu VT, Sasaki T, Maekawa Y, et al. Prenatal cranial bone development of Thomas's horseshoe bat (*Rhinolophus thomasi*): with special reference to petrosal morphology. J Morphol. 2018;279:809–27.

38. Nojiri T, Fukui D, Werneburg I, Saitoh T, Endo H, Koyabu D. Embryonic staging of bats with special reference to *Vespertilio sinensis* and its cochlear development. Dev Dyn. 2021;250:1140–59.

39. Nojiri T, Wilson LAB, López-Aguirre C, Tu VT, Kuratani S, Ito K, et al. Embryonic evidence uncovers convergent origins of laryngeal echolocation in bats. Curr Biol. 2021;31:1353-1365.e3.

40. Nojiri T, Tu VT, Sohn JH, Koyabu D. On the sequence heterochrony of cranial ossification of bats in light of Haeckel's recapitulation theory. J Exp Zool B Mol Dev Evol. 2022;338:137–48.

41. Sulser RB, Patterson BD, Urban DJ, Neander AI, Luo Z-X. Evolution of inner ear neuroanatomy of bats and implications for echolocation. Nature. 2022;602:449–54.

42. Snipes CCG, Carter RT. The hyoid as a sound conducting apparatus in laryngeally echolocating bats. J Anat. 2022;240:1020–33.

43. Simmons NB, Geisler JH. Phylogenetic relationships of Icaronycteris, Archaeonycteris, Hassianycteris, and Palaeochiropteryx to extant bat lineages, with comments on the evolution of echolocation and foraging strategies in Microchiroptera. Bulletin of the AMNH; no. 235. 1998.

44. Hand SJ, Maugoust J, Beck RMD, Orliac MJ. A 50-million-year-old, three-dimensionally preserved bat skull supports an early origin for modern echolocation. Curr Biol. 2023;33:4624–40.

45. Dobson GE. On the structure of the pharynx, larynx, and hyoid bones in the Epomophori; with remarks on its relation to the habits of these animals. Proceedings of the Zoological Society of London. 1881. p. 685–93.

46. Elias H. Zur anatomie des Kehlkopfes der Mikrochiropteren. Gegenbaurs morphologisches Jahrbuch. 1907. p. 736.

47. Sprague JM. The hyoid region of placental mammals with especial reference to the bats. Am J Anat. 1943;72:385–472.

48. Carter RT, Adams RA. Ontogeny of the larynx and flight ability in Jamaican fruit bats (Phyllostomidae) with considerations for the evolution of echolocation. Anat Rec. 2014;297:1270–7.

49. Carter RT, Adams RA. Integrating ontogeny of echolocation and locomotion gives unique insights into the origin of bats. J Mamm Evol. 2016;23:413–21.

50. Carter RT. Reinforcement of the larynx and trachea in echolocating and non-echolocating bats. J Anat [Internet]. 2020;237:495–503.

51. Snipes CCG, Carter RT. Vibroacoustic response of the tympanic membrane to hyoid-borne sound generated during echolocation in bats. Integr Org Biol. 2023;5:obad004.

52. Brualla NLM, Wilson LAB, Doube M, Carter RT, McElligott AG, Koyabu D. The vocal apparatus: an understudied tool to reconstruct the evolutionary history of echolocation in bats? J Mamm Evol. 2023;30:79–94.

53. Musolf K, Penn DJ. Ultrasonic vocalizations in house mice: a cryptic mode of acoustic communication. Evol House Mouse. 2012;3:253.

54. Metscher BD. MicroCT for developmental biology: a versatile tool for high-contrast 3D imaging at histological resolutions. Dev Dyn. 2009;238:632–40.

55. Gignac PM, Kley NJ, Clarke JA, Colbert MW, Morhardt AC, Cerio D, et al. Diffusible iodine-based contrast-enhanced computed tomography (diceCT): an emerging tool for rapid, high-resolution, 3-D imaging of metazoan soft tissues. J Anat. 2016;228:889–909.

56. Haney MM, Hamad A, Woldu HG, Ciucci M, Nichols N, Bunyak F, et al. Recurrent laryngeal nerve transection in mice results in translational upper airway dysfunction. J Comp Neurol. 2020;528:574–96.

57. Suthers RA, Fattu JM. Mechanisms of sound production by echolocating bats. Am Zool. 1973;13:1215–26.

58. Griffiths TA. Comparative laryngeal anatomy of the big brown bat, *Eptesicus fuscus*, and the Mustached bat, *Pteronotus parnellii*. Mammalia. 1983;47:377–94.

59. Robin HA. Recherches anatomiques sur les mammifères de l'ordre des chiroptères. Paris Ann Sci Nat Zool. 1881.

60. Giannini NP, Wible JR, Simmons NB. On the cranial osteology of Chiroptera. I. pteropus (megachiroptera: Pteropodidae). Bull Am Mus Nat Hist. 2006;295:1–134.

61. de Bakker BS, de Bakker HM, Soerdjbalie-Maikoe V, Dikkers FG. The development of the human hyoid-larynx complex revisited. Laryngoscope. 2018;128:1829–34.
62. Rodríguez-Vázquez JF, Kim JH, Verdugo-López S, Murakami G, Cho KH, Asakawa S, et al. Human fetal hyoid body origin revisited. J Anat. 2011;219:143–9.
63. Henick DH. Three-dimensional analysis of murine laryngeal development. Ann Otol Rhinol Laryngol Suppl. 1993;159:3–24.
64. Alli O, Berzofsky C, Sharma S, Pitman MJ. Development of the rat larynx: a histological study. Laryngoscope. 2013;123:3093–8.
65. Hast MH. Early development of the human laryngeal muscles. Ann Otol Rhinol Laryngol. 1972;81:524–30.
66. Förster G, Arnold D, Bischoff SJ, Schubert H, Scholle H-C, Müller AH. Laryngeal pacing in minipigs: in vivo test of a new minimal invasive transcricoidal electrode insertion method for functional electrical stimulation of the PCA. Eur Arch Otorhinolaryngol. 2013;270:225–31.
67. Cheetham J, Radcliffe CR, Ducharme NG, Sanders I, Mu L, Hermanson JW. Neuroanatomy of the equine dorsal cricoarytenoid muscle: surgical implications. Equine Vet J. 2008;40:70–5.
68. Mead AF, Osinalde N, Ørtenblad N, Nielsen J, Brewer J, Vellema M, et al. Fundamental constraints in synchronous muscle limit superfast motor control in vertebrates. Elife. 2017;6:e29425.
69. McKenna KZ, Wagner GP, Cooper KL. A developmental perspective of homology and evolutionary novelty. Curr Top Dev Biol. 2021;141:1–38.
70. Galis F. Key innovations and radiations. In: Wagner GP, editor. The Character Concept in Evolutionary Biology. Academic Press; 2001. p. 581–605.
71. Sekine K, Ohuchi H, Fujiwara M, Yamasaki M, Yoshizawa T, Sato T, et al. Fgf10 is essential for limb and lung formation. Nat Genet. 1999;21:138–41.
72. Bachiller D, Klingensmith J, Shneyder N, Tran U, Anderson R, Rossant J, et al. The role of chordin/Bmp signals in mammalian pharyngeal development and DiGeorge syndrome. Development. 2003;130:3567–78.
73. Tabler JM, Rigney MM, Berman GJ, Gopalakrishnan S, Heude E, Al-Lami HA, et al. Cilia-mediated Hedgehog signaling controls form and function in the mammalian larynx. Elife. 2017;6:e19153.
74. Lungova V, Verheyden JM, Sun X, Thibeault SL. β-Catenin signaling is essential for mammalian larynx recanalization and the establishment of vocal fold progenitor cells. Development. 2018;145:dev157677.
75. Adachi N, Bilio M, Baldini A, Kelly RG. Cardiopharyngeal mesoderm origins of musculoskeletal and connective tissues in the mammalian pharynx. Development. 2020;147:dev185256.
76. Novick A, et al. Pulse Duration in the Echolocation of Insects by the Bat, Pteronotus. In: Autrum H, Bünning EV, Frisch K, Hadorn E, Kühn A, Mayr E, et al., editors. Orientierung der Tiere/Animal Orientation: Symposium in Garmisch-Partenkirchen 17–21 9 1962. Berlin: Springer, Berlin Heidelberg; 1963. p. 21–6.
77. Suthers RA, Hartley DJ, Wenstrup JJ. The acoustic role of tracheal chambers and nasal cavities in the production of sonar pulses by the horseshoe bat. Rhinolophus hildebrandti J Comp Physiol A. 1988;162:799–813.
78. Rübsamen R, Schäfer M. Ontogenesis of auditory fovea representation in the inferior colliculus of the Sri Lankan rufous horseshoe bat. Rhinolophus rouxi J Comp Physiol A. 1990;167:757–69.
79. Funakoshi K, Nomura E, Matsukubo M, Wakita Y. Postnatal growth and vocalization development of the lesser horseshoe bat, Rhinolophus cornutus, in the Kyushu district. Japan jmam. 2010;35:65–78.
80. Morton ES. On the occurrence and significance of motivation-structural rules in some bird and mammal sounds. Am Nat. 1977;111:855–69.
81. Ying LIU, Feng J, Jiang YL, Sun LWKP. Vocalization development of greater horseshoe bat, *Rhinolophus ferrumequinum* (Rhinolophidae, Chiroptera). Folia Zool Brno. 2007;56:126–36.
82. Simmons NB, Seymour KL, Habersetzer J, Gunnell GF. Inferring echolocation in ancient bats. Nature. 2010. p. E8; discussion E9.
83. Carter RT, Stuckey A, Adams RA. Ontogeny of the hyoid apparatus in Jamaican fruit bats (Chiroptera: Phyllostomidae) in unraveling the evolution of echolocation in bats. J Zool. 2019;308:301–7.
84. Griffiths TA. Systematics of the New World nectar-feeding bats (Mammalia, Phyllostomidae), based on the morphology of the hyoid and lingual regions. American Museum novitates; no. 2742. 1982
85. Griffiths TA, Criley BB. Comparative lingual anatomy of the bats *Desmodus rotundus* and *Lonchophylla robusta* (Chiroptera: Phyllostomidae). J Mammal. 1989;70:608–13.
86. Romankowowa A. Comparative study of the skeleton of the hyoid apparatus in some bat species; Badania porównawcze szkieletu aparatu gnykowego u niektórych gatunków nietoperzy. Acta Theriol. 1963;7:15–23.
87. Jebb D, Huang Z, Pippel M, Hughes GM, Lavrichenko K, Devanna P, et al. Six reference-quality genomes reveal evolution of bat adaptations. Nature. 2020;583:578–84.
88. Hedges SB, Kumar S. The timetree of life. OUP Oxford. 2009.
89. Cretekos CJ, Weatherbee SD, Chen C-H, Badwaik NK, Niswander L, Behringer RR, et al. Embryonic staging system for the short-tailed fruit bat, *Carollia perspicillata*, a model organism for the mammalian order Chiroptera, based upon timed pregnancies in captive-bred animals. Dev Dyn. 2005;233:721–38.
90. Ito K, Tu VT, Eiting TP, Nojiri T. On the embryonic development of the nasal turbinals and their homology in bats. Front Cell Develop Biol. 2021;9:613545.
91. Chi T-C, Tu VT, Sohn J, Kimura J, Koyabu D. Caudal auricular muscle variations and the evolution of echolocation behavior in pteropodid bats. J Vet Med Sci. 2023;85:625–30.
92. Chi T-C, Meguro F, Takechi M, Furutera T, Tu VT, Higashiyama H, et al. Anatomy and homology of the caudal auricular muscles in greater short-nosed fruit bat (*Cynopterus sphinx*). J Vet Med Sci. 2023;85:571–7.
93. Sohn JH, Fukui D, Nojiri T, Minowa K, Kimura J. Three-dimensional and histological observations on male genital organs of greater horseshoe bat *Rhinolophus ferrumequinum*. J Mamm Evol. 2021;28:559–71.
94. Jungers WL, Falsetti AB, Wall CE. Shape, relative size, and size-adjustments in morphometrics. Am J Phys Anthropol. 1995;38:137–61.
95. Koyabu D, Werneburg I, Morimoto N, Zollikofer CPE, Forasiepi AM, Endo H, et al. Mammalian skull heterochrony reveals modular evolution and a link between cranial development and brain size. Nat Commun. 2014;5:3625.
96. Aiello WG, Freedman HI, Wu J. Analysis of a model representing stage-structured population growth with state-dependent time delay. SIAM J Appl Math. 1992;52:855–69.
97. Rayner JMV. Linear relations in biomechanics: the statistics of scaling functions. J Zool. 1985;206:415–39.
98. Nelder JA, Wedderburn RWM. Generalized linear models. J R Stat Soc Ser A. 1972;135:370.

Publisher's Note